Article

Application of MCD Spectroscopy and TD–DFT to a Highly Non-Planar Porphyrinoid Ring System. New Insights on Red–Shifted Porphyrinoid Spectral Bands

John Mack, Yoshiaki Asano, Nagao Kobayashi, and Martin J. Stillman

J. Am. Chem. Soc., **2005**, 127 (50), 17697-17711• DOI: 10.1021/ja0540728 • Publication Date (Web): 25 November 2005

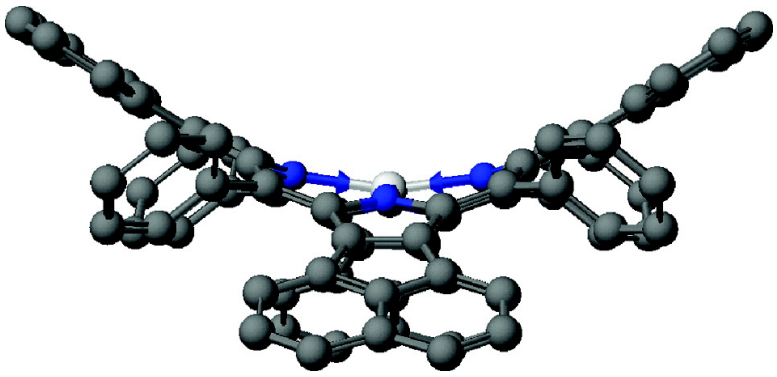

More About This Article

Additional resources and features associated with this article are available within the HTML version:

- Supporting Information
- Links to the 14 articles that cite this article, as of the time of this article download
- Access to high resolution figures
- Links to articles and content related to this article
- Copyright permission to reproduce figures and/or text from this article

View the Full Text HTML

J|A|C|S
ARTICLES
Published on Web 11/25/2005

Application of MCD Spectroscopy and TD−DFT to a Highly Non-Planar Porphyrinoid Ring System. New Insights on Red−Shifted Porphyrinoid Spectral Bands

John Mack,[†,‡] Yoshiaki Asano,[‡] Nagao Kobayashi,*[,‡] and Martin J. Stillman*[,†]

Contribution from the Department of Chemistry, University of Western Ontario, London, Ontario, Canada, N6A 5B7 and Department of Chemistry, Graduate School of Science, Tohoku University, Sendai 980-8578, Japan

Received June 20, 2005; E-mail: stillman@uwo.ca; nagaok@mail.tains.tohoku.ac.jp

Abstract: The first magnetic circular dichroism (MCD) spectra are reported for tetraphenyltetraacenaphthoporphyrin (TPTANP). The impact on the electronic structure of steric interactions between the fused acenaphthalene rings and the *meso*-tetraphenyl substituents is explored based on an analysis of the optical spectra of the Zn(II) complex (ZnTPTANP) and the free base dication species ($[H_4TPTANP]^{2+}$). In the case of ZnTPTANP, significant folding of the porphyrinoid ligand induces a highly unusual MCD−sign reversal providing the first direct spectroscopic evidence of ligand nonplanarity. Density functional theory (DFT) geometry optimizations for a wide range of Zn(II) porphyrinoids based on the B3LYP functional and TD−DFT calculations of the associated UV−visible absorption spectra are reported, allowing a complete assessment of the MCD data. TPTANP complexes are found to fall into a class of cyclic polyenes, termed as soft MCD chromophores by Michl (*J. Pure Appl. Chem.* **1980**, *52*, 1549.), since the signs of the Faraday $\mathscr{A}_1$ terms observed in the MCD spectrum are highly sensitive to slight structural changes. The origin of an unusually large red shift of the main B (or Soret) band of MTPTANP (the most red shifted ever reported for fused-ring-expanded metal porphines) and of similar red shifts observed in the spectra of other peripherally crowded porphyrinoid complexes is also explored and explained on this basis.

Introduction

Metal porphyrin complexes play a vital role in biological redox processes such as photosynthesis and respiration.[1] The introduction of nonplanar conformations[2,3] to the heteroaromatic π−system of the porphyrin ligand is believed to play a key role in the biological function of proteins such as hemes[4] and cofactor F430 of methyl reductase.[5] Saddled and ruffled dodecasubstituted, S_4 symmetry, porphyrin complexes, have been used as model complexes[6] for porphyrin nonplanarity. A number of different techniques, including UV−visible absorption, resonance Raman, NMR, and EPR spectroscopy[2] and electrochemistry,[6d] have been used to investigate the effects of ligand folding on the electronic structure. There has been considerable recent controversy over the origins of significant red shifts observed in the major $\pi \rightarrow \pi^*$ bands of peripherally crowded dodecasubstituted porphyrins.[6,9] In this paper, we use magnetic circular dichroism spectroscopy (MCD),[7,8] and B3LYP based density functional theory (DFT) calculations to examine the degree of nonplanarity in the structure of zinc tetraphenyltetraacenaphthoporphyrin (ZnTPTANP), Figure 1, and the impact of ligand folding on the orbital angular momentum (OAM) properties of the frontier molecular orbitals (MOs) of the π−system. The complex band morphology of MCD spectra

[†] University of Western Ontario.
[‡] Tohoku University.

(1) (a) *The Porphyrins*; Dolphin, D., Ed.; Academic Press: New York, 1978. (b) *Ann. New York Acad. Sci*. **1973**, 206. (c) *The Porphyrin Handbook*; Kadish, K. M., Smith, K. M., Guilard, R., Eds.; Academic Press: New York, 1999.
(2) Shelnutt, J. A.; Song, X.-Z.; Ma, J.-G.; Jia, S.-L.; Jentzen, W.; Medforth, C. *J. Chem. Soc. Rev.* **1998**, *27*, 31−42.
(3) Barkigia, K. M.; Chantranupong, L.; Smith K. M.; Fajer, J. *J. Am. Chem. Soc.* **1988**, *110*, 7566−7567.
(4) Crane, B. R.; Siegel, L. M.; Getzoff, E. D. *Science* **1995**, *270*, 59−67.
(5) (a) Zimmer, M.; Crabtree, R. H. *J. Am. Chem. Soc.* **1990**, *112*, 1062−1066. (b) Furenlid, D. E.; Renner, M. W.; Smith, K. M.; Fajer, J. *J. Am. Chem. Soc*. **1990**, *112*, 1634−1635. (c) Furenlid, D. E.; Renner, M. W.; Fajer, J. *J. Am. Chem. Soc.* **1990**, *112*, 8987−8989.
(6) (a) Haddad, R. E.; Gazeau, S.; Pécaut, J.; Marchon, J.-C.; Medforth, C. J. Shelnutt, J. A. *J. Am. Chem. Soc.* **2003**, *125*, 1253−1268. (b) Shelnutt J. A.; et al. *J. Porphyrins Phthalocyanines* **2004**, *8*, 487. (c) Shelnutt, J. A.; et. al. *Inorg. Chem.* **2003**, *42*, 2227−2241. (d) Kadish, K. M.; et al. *Inorg. Chem*. **2002**, *41*, 6673−6687. (e) Medforth, C. J.; Senge, M. O.; Smith, K. M.; Sparks, L. D.; Shelnutt, J. A. *J. Am. Chem. Soc.* **1992**, *114*, 9859−9869. (f) Senge, M. O.; Medforth, C. J.; Sparks, L. D.; Shelnutt, J. A.; Smith, K. M. *Inorg. Chem.* **1993**, *32*, 1716−1723. (g) Medforth, C. J.; Senge, M. O.; Forsyth, T. P.; Hobbs, J. D.; Shelnutt, J. A.; Smith, K. M. *Inorg. Chem*. **1994**, *33*, 3865−3872. (h) Hobbs, J. D.; Majumber, S. A.; Luo, L.; Sickelsmith, G. A.; Medforth, C. J.; Smith, K. M.; Shelnutt, J. A. *Inorg. Chem.* **1994**, *33*, 3865−3872. (i) Senge, M. O.; Medforth, C. J.; Forsyth, T. P.; Lee, D. D.; Olmstead, M. M.; Jentzen, W.; Pandey, R. K.; Shelnutt, J. A.; Smith, K. M. *Inorg. Chem.* **1997**, *36*, 1149−1163. (j) Holten, D.; et al. *J. Am. Chem. Soc.* **1998**, *120*, 3781−3791. (k) Nelson, N. Y.; Medforth, C. J.; Nurco, D. J.; Jia, S.-L.; Shelnutt, J. A.; Smith, K. M. *Chem. Commun.* **1999**, 2071−2072. (l) Muzzi, C. M.; Medforth, C. J.; Voss, L.; Cancilla, M.; Lebrilla, C.; Ma, J.-G.; Shelnutt, J. A.; Smith, K. M. *Tetrahedron Lett.* **1999**, *40*, 6159−6162.
(7) Gouterman, M. In *The Porphyrins*; Dolphin, D., Ed.; Academic Press: New York, 1978; Vol. III, Part A, pp 1−165.
(8) (a) Mack, J.; Stillman, M. J. In *Handbook of Porphyrins and Related Macrocycles*; Kadish, K., Smith, K., Guilard, R., Eds.; Academic Press: New York, 2003; Vol. 16, Ch. 103, pp 43−116. (b) Mack, J.; Stillman, M. J. *Coord. Chem Rev.* **2001**, *219*−*221*, 993−1032.
(9) Ryeng, H.; Ghosh, A. *J. Am. Chem. Soc.* **2002**, *124*, 8099−8103. (b) Wertsching, A. K.; Koch, A. S.; Di Magno, S. G. *J. Am. Chem. Soc.* **2001**, *123*, 3932−3939. (c) Di Magno, S. G. *J. Porphyrins Phthalocyanines* **2004**, *8*, 523. (d) Di Magno, S. G.; Wertsching, A. K.; Ross, C. R., II *J. Am. Chem. Soc.* **1995**, *117*, 8279−8280.

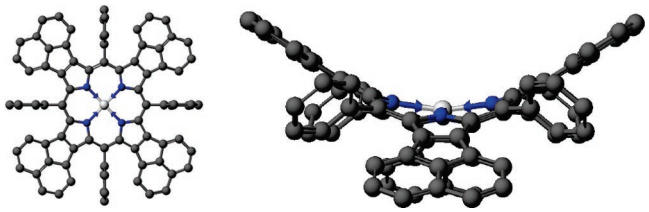

Figure 1. Molecular structures of zinc tetraphenyltetraacenaphthoporphyrin (TPTANP) in a planar D_{4h} model structure (LEFT) and in the saddled S_4 geometry (RIGHT) predicted based on B3LYP DFT geometry optimizations.

provide ground and excited-state degeneracy and spectral band polarization information that cannot be derived from the analysis of TD−DFT calculations and of UV−visible absorption spectra alone.

Lash has reported that the UV−visible spectrum of TPTANP complexes, Figure 1, contain the most substantial red shift of the B (or Soret) band ever observed for a porphyrinoid complex (to ∼558 nm in the case of ZnTPTANP).[10] The steric interactions between peripherally fused acenaphthalene rings and the phenyl substituents of MTPTANP complexes are directly analogous to those between the substituents of sterically hindered dodecasubstituted porphyrins. Molecular modeling calculations predicted that steric interactions between the phenyl substituents and the peripherally fused acenaphthalenes force the π−system to adopt a highly saddled S_4 structure similar to those reported for dodecasubstituted porphyrins, Figure 1. When no temperature dependence was observed in the NMR spectra of MTPTANP, the data were interpreted in terms of a "frozen" deep saddle configuration.[10b] Since this reported lack of temperature dependence is potentially consistent with either a saddled S_4 or a planar D_{4h} symmetry, there is currently no direct unambiguous spectroscopic evidence for ligand saddling. Although in most instances UV−visible absorption spectroscopy is based primarily on the coupling of the ground and excited states by electric dipole moments and a linear redistribution of charge along the *x*-, *y*-, or *z*-axes, in the case of planar porphyrinoids, induced magnetic dipole moments are also a significant factor since electronic excitation results in both a linear and a circular redistribution of charge within the heteroaromatic π−system. In this paper, we explore the impact of nonplanarity on the magnetic moments induced within porphyrinoid excited states with reference to trends in the UV−visible absorption and MCD spectral data for the series of Zn(II) porphyrinoid complexes shown in Figure 2, and in calculated UV−visible absorption spectra obtained from time-dependent DFT (TD−DFT) and INDO/s calculations based on a set of DFT geometry optimizations with the B3LYP functional. Zn(II) complexes are ideal for studying trends in the wavelengths and intensities of the $\pi \rightarrow \pi^*$ bands of porphyrinoid ligands, since the central metal has a closed shell d^{10} configuration. Liao and Scheiner[11] have recently demonstrated, based on Vosko, Wilk, and Nusair (VWN) DFT calculations of Fe, Co, Ni, Cu, Zn, and Mg phthalocyanine, that the 3d orbitals of Zn(II) are located deep enough energetically that there is no charge-transfer contribution in the UV−visible region as had already been deduced empirically based on analysis of electrochemical and optical data.[8,12] Calculated TD−DFT based UV−visible absorption spectra have been reported previously by Pachter and co-workers[13] for ZnP, ZnTPP, ZnTBP, and ZnPc based on DFT geometry optimizations with B3LYP. The application of DFT techniques to magnetic dipole moment based properties such as MCD spectroscopy[14] has still to be fully developed, however. Theoretical approaches, based on semiempirical theoretical techniques, such as Michl's perimeter model[15] and Gouterman's 4-orbital model,[13,16] therefore, continue to play an important role in the interpretation of the optical spectra of porphyrinoids.

We report that MCD spectra for ZnTPTANP are markedly different from those of the Zn(II) analogous complexes of tetraphenyltetrabenzoporphyrin (ZnTPTBP)[17] and the saddled D_{2d} symmetry octa-α-phenylphthalocyanine ($(\alpha C_6H_5)_8Pc$), for which positive Faraday $\mathscr{A}_1$ terms are the dominant spectral feature.[18] In contrast, the spectrum of ZnTPTANP is similar to those of chlorin complexes,[19] such as the chlorophylls,[19d] where the negative Faraday $\mathscr{A}_1$ term pattern is observed in pairs of coupled oppositely signed Faraday $\mathscr{B}_0$ terms. The MCD spectral properties and the unusually large red shift of the B band of MTPTANP reported by Lash[10] can be readily accounted for based on the trends predicted in the energies of the four frontier MOs of the porphyrinoid π−systems in Figure 2 and the application of Michl's perimeter model[15] and Gouterman's 4−orbital model to the results obtained from B3LYP geometry optimizations and TD−DFT calculations.[13,16]

Materials and Methods

(a) Zinc Tetraphenyltetraacenaphthoporphyrin. A mixture of tetraphenyltetraacenaphthoporphyrin (20 mg, 0.018 mmol) and zinc acetate dihydrate (118 mg, 0.54 mmol) was refluxed in methylene chloride−ethanol (3:2 v/v) (3 mL) in the dark for ca. 12 h. After evaporation of the solvent, the residue was imposed on an alumina column using toluene containing 2−3%

(10) (a) Lash, T. D.; Chandrasekar, P. *J. Am. Chem. Soc.* **1996**, *118*, 8767−8768. (b) Spence, J. D.; Lash, T. D. *J. Org. Chem.* **2000**, *65*, 1530−1539. (c) Lash, T. D. In *The Porphyrin Handbook*; Kadish, K. M., Smith, K. M., Guilard, R., Eds.; Academic Press: New York, 1999; Vol. II, Ch. 10, pp 125−199. (d) Lash, T. D. *J. Porphyrins Phthalocyanines* **2001**, *5*, 267−288.

(11) Liao, M.-S.; Scheiner, S. *J. Chem. Phys.* **2001**, *114*, 9780−9791.

(12) (a) Stillman, M. J.; Nyokong, T. In *Phthalocyanine. Principles and Properties*; Leznoff, C. C., Lever, A. B. P., Eds.; VCH Publications: New York, 1993; Vol. 1, Ch. 3, pp 133−290. (b) Stillman, M. J. In *Phthalocyanine. Principles and Properties*; Lever A. B. P., Leznoff, C. C., Eds.; VCH Publications: New York, 1993; Part III, Ch. 5, pp 227−296.

(13) (a) Nguyen, K. A.; Pachter, R. *J. Chem. Phys.* **2001**, *114*, 10757−10767. (b) Nguyen, K. A.; Day, P. N.; Pachter, R.; Tretiak, S.; Chernyak, V.; Mukamel, S. *J. Phys. Chem. A* **2002**, *106*, 10285−10293.

(14) (a) Autschbach, J.; Ziegler, T. *J. Chem. Phys.* **2002**, *116*, 891−896. (b) Seth, M.; Ziegler, T.; Banerjee, A.; Autschbach, J.; van Gisbergen, S. J. A.; Baerends, E. J. *J. Chem. Phys.* **2004**, *120*, 10942−10954.

(15) (a) Michl, J. *J. Am. Chem. Soc.* **1978**, *100*, 6801−6811. (b) Michl, J. *J. Am. Chem. Soc.* **1978**, *100*, 6812−6818. (c) Michl, J. *J. Am. Chem. Soc.* **1978**, *100*, 6819−6824. (d) Michl, J. *Pure Appl. Chem.* **1980**, *52*, 1549−1563.

(16) (a) Weiss, C., Jr. *J. Mol. Spectrosc.* **1972**, *44*, 37−80. (b) Gouterman, M.; Wagniere, G. H.; Snyder, L. C. *J. Mol. Spectrosc.* **1963**, *11*, 108−127. (c) Weiss, C., Jr.; Kobayashi, H.; Gouterman, M. *J. Mol. Spectrosc.* **1965**, *16*, 415−450. (d) McHugh, A. J.; Gouterman, M.; Weiss, C., Jr. *Theor. Chim. Acta* **1972**, *24*, 346−370. (e) Schaffer, A. M.; Gouterman, M.; Davidson, E. R. *Theor. Chim. Acta* **1973**, *30*, 9−30.

(17) Luk'yanets, E. A.; Dashkevich, S. N.; Kobayashi, N. *Russ. J. Gen. Chem.* **1993**, *63*, 985−988.

(18) (a) Kobayashi, N.; Fukuda, T.; Ueno, K.; Ogino, H. *J. Am. Chem. Soc.* **2001**, *123*, 10740−10741. (b) Fukuda, T.; Homma, S.; Kobayashi, N. *Chem. Commun.* **2003**, 1574−1575. (c) Fukuda, T.; Ishiguro, T. Kobayashi, N. *Tetrahedron Lett.* **2005**, *46*, 2907−2909. (d) Fukuda, T. M. Sc. Thesis, Tohoku University 2000. (e) Fukuda, T.; Ono, K.; Homma, S.; Kobayashi, N. *Chem. Lett.* **2003**, *32*, 736−737. (f) Homma, S.; Fukuda, T.; Kobayashi, N. *J. Porphyrins Phthalocyanines* **2004**, *8*, 691.

(19) (a) Keegan, J. D.; Stolzenberg, A. M.; Lu, Y. C.; Linder, R. E.; Barth, G.; Moscowitz, A.; Bunnenberg, E.; Djerassi, C. *J. Am. Chem. Soc.* **1982**, *104*, 4305−4317. (b) Keegan, J. D.; Stolzenberg, A. M.; Lu, Y. C.; Linder, R. E.; Barth, G.; Moscowitz, A.; Bunnenberg, E.; Djerassi, C. *J. Am. Chem. Soc.* **1982**, *104*, 4317−4329. (c) Djerassi, C.; et al. *J. Am. Chem. Soc.* **1984**, *106*, 4241−4258. (d) Houssier, C.; Sauer, K. *J. Am. Chem. Soc.* **1970**, *92*, 779−791.

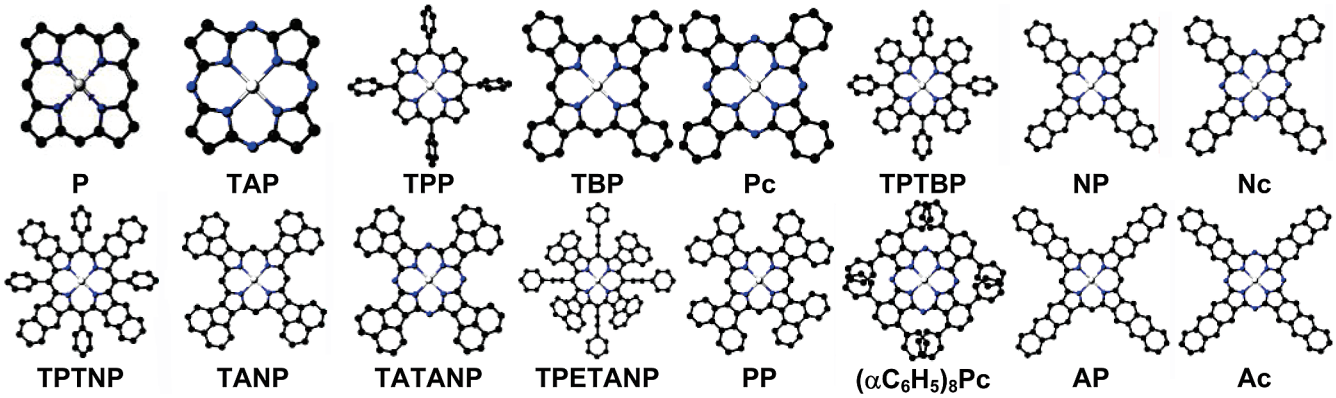

Figure 2. Molecular structures of the zinc complexes of porphyrin (P), tetraazaporphyrin (TAP), tetraphenyl-porphyrin (TPP), tetrabenzoporphyrin (TBP), phthalocyanine (Pc), tetraphenyltetrabenzoporphyrin (TPTBP), naphthoporphyrin (NP), naphthalocyanine (Nc), tetraphenyltetranaphthoporphyrin (TPTNP), tetraacenaphthoporphyrin (TANP), tetraacenaphthotetraazaporphyrin (TATANP), tetraphenyltetraacenaphthoporphyrin (TPTANP), tetraphenylethynylacenaphthoporphyrin (TPETANP), tetraphenanthroporphyrin (PP), octa-α-phenylphthalocyanine ($(\alpha C_6H_5)_8Pc$), anthracoporphyrin (AP) and anthracocyanine (Ac) based on DFT geometry optimizations using the B3LYP functional of the Gaussian 03 program with 6−31G basis sets.[21]

pyridine as the eluent. After evaporation of the solvent, the resulting dark purple solid was recrystalized from methylene chloride-methanol to give 11 mg of ZnTPTANP. Anal. Found: C, 81.82; H, 3.88; N, 5.29%. Calcd. for $C_{84}H_{44}N_4Zn.C_6H_5N^+$-$CH_3COO^-$: C, 83.41; H, 3.96; N, 5.29%. A parent peak with m/z = 1172.3 was obtained from ESI−MS recorded on a chloroform solution matching the anticipated mass for $C_{84}H_{44}N_4$-Zn of 1172.8. Metal free TPTANP was synthesized according to the literature.[10] Anal. Found: C, 89.86; H, 4.53; N, 4.74%. Calcd for $C_{84}H_{46}N_4$: C, 90.79; H, 4.17; N, 5.04.

(b) Optical Spectroscopy. Absorption spectra were recorded with a Cary 500 spectrophotometer. MCD spectra were recorded at room temperature on a Jasco J-810 spectrometer with a field of 4.3 T from an Oxford Instruments SM2 superconducting magnet. The field strength and sign were calibrated by measuring the MCD spectrum of an aqueous solution of CoSO4 at 510 nm ($\Delta\epsilon_M$ = −1.8969 L mol^{-1} cm^{-1} T^{-1}). The signal intensity of the CD spectrometer was also tested using ammonium d-camphor-10-sulfonate to ensure that the θ°/A ratio for the peaks at 280 nm was 2.26.[20] Steady-state emission spectra were measured with a Photon Technology Quanta Master (QM4/2003) scanning spectrofluorometer using a Xe flash lamp with an excitation wavelength of 545 and 555 nm for ZnTPTANP and $[H_4TPTANP]^{2+}$ in CH_2Cl_2, respectively.

(c) Molecular Orbital Calculations. Molecular structures were refined for a wide range of zinc porphyrinoid complexes, Figure 2, through the use of the Gaussian 03[21] and the CACheworkstation (Fujitsu America Inc.)[22] software packages. Structures were optimized using the B3LYP functional within Gaussian 03 with 6−31G and 6−31G(d) basis sets.[23] UV−visible absorption spectra were calculated using TD−DFT on Gaussian 03 with 6−31G and 6−31G(d) basis sets and by using the ZINDO/s calculation[24] on the CACheworkstation based on all the MOs from HOMO−25 to LUMO+25. Pachter[13a] has demonstrated that the differences obtained in TD−DFT results for ZnP calculations with 6−31G(d), 6-31+G(d) and 6-311+G-(d) basis sets are very minor. We performed B3LYP geometry optimizations for the Zn(II) complexes in Figure 2 using both 6−31G and 6−31G(d) basis sets. Since only minor differences were observed, 6−31G basis sets were used to calculate a series of TD−DFT calculated spectra into the UV-region including the more computationally demanding complexes such as ZnTPETANP and $Zn(\alpha C_6H_5)_8Pc$. ZnTPTBP, ZnTPTNP, ZnTPTANP, and ZnTPETANP, Figure 2, are predicted to be saddled into nonplanar S_4 structures, Tables 1 and S1, while PP and $(\alpha C_6H_5)_8Pc$ complexes are saddled into D_{2d} structures. A D_{4h} ZnTPTANP model geometry was constructed based on phenylation of a locked optimized ZnTANP structure using the MOPAC 2002 program within the CACheworkstation.[22b]

MCD Spectroscopy. MCD spectroscopy[25] can be used to derive structural information from the Zeeman splitting of electronic states that cannot be obtained from UV−visible absorption and NMR spectra. Analysis of the MCD spectrum is based on MCD intensity mechanisms described in the Faraday $\mathscr{A}_1$, $\mathscr{B}_0$, and $\mathscr{C}_0$ terms, (see Supporting Information) Platt,[26a] Moffitt,[26b] and Michl[15] demonstrated that the relative intensities

(20) Chen, G. C.; Yang, J. T. *Anal. Lett.* **1977**, *10*, 1195−1207.
(21) Frisch, M. J.; Trucks, G. W.; Schlegel, H. B.; Scuseria, G. E.; Robb, M. A.; Cheeseman, J. R.; Montgomery, J. A., Jr.; Vreven, T.; Kudin, K. N.; Burant, J. C.; Millam, J. M.; Iyengar, S. S.; Tomasi, J.; Barone, V.; Mennucci, B.; Cossi, M.; Scalmani, G.; Rega, N.; Petersson, G. A.; Nakatsuji, H.; Hada, M.; Ehara, M.; Toyota, K.; Fukuda, R.; Hasegawa, J.; Ishida, M.; Nakajima, T.; Honda, Y.; Kitao, O.; Nakai, H.; Klene, M.; Li, X.; Knox, J. E.; Hratchian, H. P.; Cross, J. B.; Bakken, V.; Adamo, C.; Jaramillo, J.; Gomperts, R.; Stratmann, R. E.; Yazyev, O.; Austin, A. J.; Cammi, R.; Pomelli, C.; Ochterski, J. W.; Ayala, P. Y.; Morokuma, K.; Voth, G. A.; Salvador, P.; Dannenberg, J. J.; Zakrzewski, V. G.; Dapprich, S.; Daniels, A. D.; Strain, M. C.; Farkas, O.; Malick, D. K.; Rabuck, A. D.; Raghavachari, K.; Foresman, J. B.; Ortiz, J. V.; Cui, Q.; Baboul, A. G.; Clifford, S.; Cioslowski, J.; Stefanov, B. B.; Liu, G.; Liashenko, A.; Piskorz, P.; Komaromi, I.; Martin, R. L.; Fox, D. J.; Keith, T.; Al-Laham, M. A.; Peng, C. Y.; Nanayakkara, A.; Challacombe, M.; Gill, P. M. W.; Johnson, B.; Chen, W.; Wong, M. W.; Gonzalez, C.; Pople, J. A. Gaussian *03*, revision C.02; Gaussian, Inc.: Wallingford, CT, 2004.
(22) (a) CACheScientific P.O. Box 500, Mail Station 13−400 Beaverton, OR 97077. (b) Stewart, J. J. P. MOPAC 2002, Fujitsu Limited, Tokyo, Japan, 1999.
(23) (a) Stratmann, R. E.; Scuseria, G. E.; Frisch, M. J. *J. Chem. Phys.* **1988**, *109*, 8218−8224. (b) Bauernschmitt, R.; Ahlrichs, R. *Chem. Phys. Lett.* **1996**, *256*, 454−464. (c) Casida, M. E.; Jamorski, C.; Casida, K. C.; Salahub, D. R. *J. Chem. Phys.* **1988**, *108*, 4439−4449.
(24) (a) Ridley, J. E.; Zerner, M. C. *Theor. Chim. Acta* **1973**, *32*, 111−134. (b) Zerner, M. C.; Loew, G. H.; Kirchner, R. F.; Mueller-Westerhoff, U. T. *J. Am. Chem. Soc.* **1980**, *102*, 589−599. (c) Ridley, J. E.; Zerner, M. C. *Theor. Chim. Acta* **1976**, *42*, 223−236. (d) Bacon, A.; Zerner, M. C. *Theor. Chim. Acta* **1979**, *53*, 21−54. (e) Head, J.; Zerner, M. C. *Chem. Phys. Lett.* **1985**, *122*, 264−270. (f) Head, J.; Zerner, M. C. *Chem. Phys. Lett.* **1986**, *131*, 359−366. (g) Anderson, W.; Edwards, W. D.; Zerner, M. C. *Inorg. Chem.* **1986**, *25*, 2728−2732. (h) Edwards, W. D.; Zerner, M. C. *Theor. Chim. Acta* **1987**, *72*, 347−361. (i) Kotzian, M.; Roesch, N.; Zerner, M. C. *Theor. Chim. Acta* **1992**, *81*, 201−222. (j) Kotzian, M.; Roesch, N.; Zerner, M. C. *Int. J. Quantum Chem., Quantum Chem. Symp.* **1991**, *25*, 545−555.
(25) (a) Piepho, S. B.; Schatz, P. N. In *Group Theory in Spectroscopy with Applications to Magnetic Circular Dichroism*; Wiley: New York, 1983. (b) Stephens, P. *J. Adv. Chem. Phys.* **1976**, *35*, 197−264. (c) Buckingham, A. D.; Stephens, P. *J. Annu. Rev. Phys. Chem.* **1966**, *17*, 399−432.

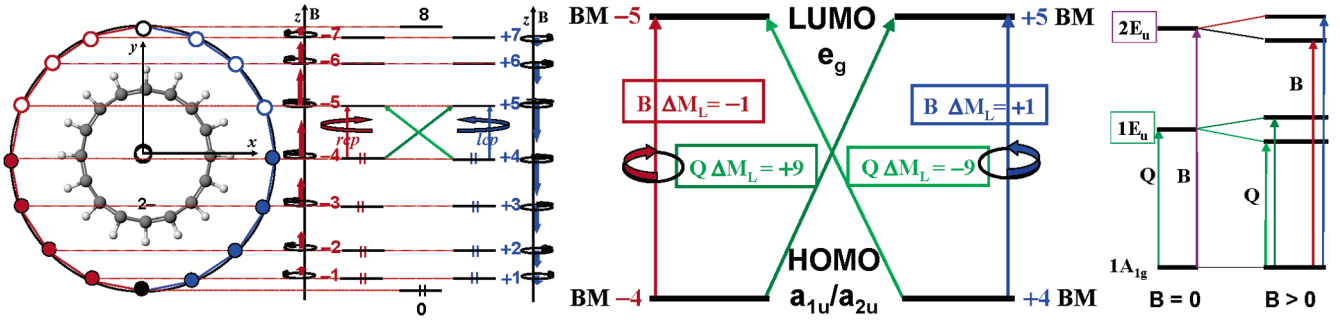

Figure 3. Michl's perimeter model for $C_{16}H_{16}^{2-}$ (LEFT). The circle represents a diagrammatic representation of the clockwise and counterclockwise motion of π-system electrons on the inner ligand perimeter generating the M_L value for each complex π-MO. The alignment and magnitude of the magnetic moments induced by the electron motion within each π-MO (CENTER) can be predicted based on the right-hand rule and LCAO calculations.[7,15c,16d] The moments are shown diagrammatically. Right and left-handedness is defined within classical optics looking toward the light source of the CD spectrometer. The origin of the Q and B bands in Gouterman's 4-orbital LCAO model (CENTER and RIGHT).

of the major electronic bands within the optical spectra of aromatic $\pi-$systems, can be successfully described in terms of a perimeter model based on a high-symmetry parent hydrocarbon ($C_{16}H_{16}^{2-}$ in the case of the inner cyclic perimeter tetrapyrrole porphyrinoid complexes), since the nodal patterns of the $\pi-$system MOs are retained even when the symmetry of the cyclic perimeter is substantially modified, Figures 3 and S1.[7] An $M_L = 0, \pm1, \pm2, \pm3, \pm4, \pm5, \pm6, \pm7, 8$ sequence of MOs is formed in ascending energy in the case of metal porphyrinoid complexes in an analogous manner to the $M_L = 0, \pm1, \pm2, 3$ $\pi-$MO sequence that is responsible for the aromaticity of benzene. The incorporation of the four pyrrole rings reduces the symmetry of porphyrinoids from D_{16h} to D_{4h}. The orbitally degenerate LUMO ($1e_g^*$) has $M_L = \pm5$ nodal patterns, while the HOMOs ($1a_{1u}$ and $1a_{2u}$) have an $M_L = \pm4$ nodal patterns and remain accidentally near degenerate. Within the band nomenclature of Gouterman's 4-orbital model,[7,16] Figure 3, there is an allowed B transition and a forbidden Q transition with $\Delta M_L = \pm1\ \beta$ and $\pm9\ \beta$, respectively. Since the magnetic and electric vectors of electromagnetic radiation can rotate a maximum of once per wavelength, only $\Delta M_L = 0, \pm1$ transitions are electric dipole allowed. MCD spectroscopy confirmed the allowed and forbidden nature of the Q and B bands of MP, since $\mathscr{A}_1/\mathscr{D}_0$ ratios[27] (the Faraday $\mathscr{A}_1$ term magnitude divided by the dipole strength of the corresponding absorption band) provide a direct spectral measurement of the induced magnetic moments of the $\pi\pi^*$ excited states. The magnetic dipole values obtained are typically significantly lower than the ±1, ±9 β values predicted based on a simple free electron model for the ideal $C_{16}H_{16}^{2-}$ perimeter. Gouterman[7,16d,e] and Michl[15a] successfully used quantitative approaches based on Pariser−Parr−Pople[16d] and LCAO[15a] calculations to account for values of between −6 and −7 β, that had been reported[16d] for the excited-state magnetic moments associated with the Q band of main group and closed shell d^{10} metal porphyrins. Subsequent MO calculations[28] using techniques such as DFT have provided more accurate descriptions of the groundstate geometry but have not enhanced the basic conceptual approach for describing the relative intensities of the major $\pi \rightarrow \pi^*$ bands within ***both*** the electronic absorption and MCD spectra. Absorption of a photon by a cyclic $\pi-$system results in both a linear and a circular redistribution of charge, resulting in an electric dipole polarized along the *x*-, or *y*-axis and a magnetic moment perpendicular to the *xy*−plane. The alignment of the magnetic moments associated with the absorption of left and right circularly polarized light (*lcp* and *rcp*) is determined by the OAM associated with electron circulation on the cyclic perimeter within the ground and excited states. After electronic excitation the motion of the electron within the LUMO is no longer fully balanced by that of an electron within an MO of the opposing handedness, Figure 3. Since MCD intensity is based on the differential absorbance of *lcp* and *rcp* (ΔA_{l-r}), a Zeeman splitting of states within an applied field results in a derivative-shaped Faraday $\mathscr{A}_1$ term. For perimeters in which OAM is greater within the excited state than in the ground state, as is normally the case for metal porphyrinoids, a negative particle is effectively formed on the perimeter due to electron motion within the LUMO, which induces a negative magnetic moment value and a positive Faraday $\mathscr{A}_1$ term (a −ve/+ve sequence in ascending energy terms) within the MCD spectrum. The microstate associated with absorption of *rcp* is stabilized due to the alignment of the induced magnetic moment with the applied field within the sample bore of the superconducting magnet.

D_{4h} symmetry porphyrinoid complexes of main group and closed shell d^{10} metals have nondegenerate ground−states ($^1A_{1g}$), Figure 4. Faraday $\mathscr{A}_1$ terms with *x*/*y*-polarization dominate the MCD spectra, since the optically accessible $\pi\pi^*$ excited states remain orbitally degenerate (^1E_u).[7,8] If a structural perturbation removes the main 4-fold axis of symmetry the OAM associated with the inner perimeter is partially quenched and Gaussian-shaped Faraday $\mathscr{B}_0$ terms replace the derivative-shaped Faraday $\mathscr{A}_1$ terms. B3LYP geometry optimizations predict that an S_4 improper rotation axis is retained in the case of ZnTPTANP despite the saddling perturbation to the structure, Figure 1 and Table 1. The LUMO therefore remains orbitally degenerate, while accidental near degeneracy is predicted for the HOMOs

(26) (a) Platt, J. R. *J. Chem. Phys.* **1949**, *17*, 484−495. (b) Moffitt, W. *J. Chem. Phys.* **1954**, *22*, 320−333.
(27) Briat, B.; Schooley, D. A.; Records, R.; Bunnenberg, E.; Djerassi, C. *J. Am. Chem. Soc.* **1967**, *89*, 7062−7071.
(28) (a) Henriksson, A.; Roos, B.; Sundbom, M. *Theor. Chim. Acta* **1972**, *27*, 303−313. (b) Dedieu, A.; Rohmer, M.-M.; Veillard, A. *Adv. in Quantum Chem.* **1982**, *16*, 43−95. (c) Orti, E.; Bredas, J. L.; Clarisse, C. *J. Chem. Phys.* **1990**, *92*, 1228−1235. (d) Liang, X. L.; Flores, S.; Ellis, D. E.; Hoffman, B. M.; Musselman, R. L. *J. Chem. Phys.* **1991**, *95*, 403−417. (e) Rosa, A.; Baerends, E. J. *Inorg. Chem.* **1992**, *31*, 4717−4726. (f) Rosa, A.; Baerends, E. J. *Inorg. Chem.* **1994**, *33*, 584−595. (g) Ishikawa, N.; Ohno, O.; Kaizu, Y.; Kobayashi, H. *J. Phys. Chem.* **1992**, *96*, 8832−8839. (h) Ishikawa, N.; Ohno, O.; Kaizu, Y. *J. Phys. Chem.* **1993**, *97*, 1004−1010. (i) Ricciardi, G.; Rosa, A.; Barends, E. J. *J. Phys. Chem. A* **2001**, *105*, 3311−3327. (j) Ricciardi, G.; Rosa, A.; Barends, E. J. *J. Phys. Chem. A* **2001**, *105*, 5242−5254. (k) Baerends, E. J.; Ricciardi, G.; Rosa, A.; van Gisbergen, S. J. A. *Coord. Chem. Rev.* **2002**, *230*, 5−27.

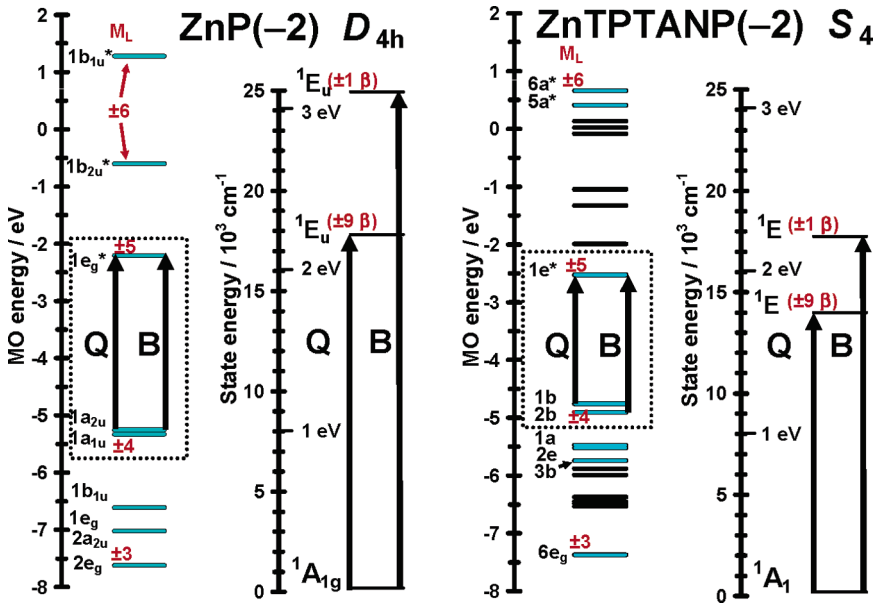

Figure 4. MO and state level diagrams for ZnP and ZnTPTANP. The MO and state orderings are based on B3LYP and TD−DFT calculations, however, they follow closely the orderings first proposed for P by Gouterman.[16e] The dotted line indicates the 4 frontier π-MOs within Gouterman's 4-orbital model,[7]Figure 3. Blue lines highlight MOs with the same nodal patterns as ZnP MOs associated primarily with the inner ligand perimeter. The values in red for OAM based properties are based on a simple free electron.

Table 1. Central Cavity Geometry and Predicted Degree of Ligand Folding for TANP, TPTANP, and TPETANP Based on Geometry Optimizations Using the B3LYP Functional with 6−31G Basis Sets

	sym[a]	N–Zn–N (Å, deg)[b]		C–Zn–C (Å, deg)[c]		N–C (Å)[d]	N–N–C (deg)[e]
TANP	D_{4h}	4.13, 4.13	0.07, 0.08	6.92, 6.92	0.09, 0.07	5.79, 5.79, 5.79, 5.79	0.02, 0.03, 0.14, 0.03
TPTANP	S_4	4.05, 4.05	4.21, 4.45	6.87, 6.87	0.09, 0.08	5.77, 5.77, 5.77, 5.77	18.88, 18.87, 18.79, 18.77
TPETANP	S_4	4.03, 4.03	5.05, 5.32	6.85, 6.85	0.02, 0.16	5.76, 5.76, 5.76, 5.76	18.87, 19.11, 18.83, 18.77

[a] Symmetry of the complex. [b] The distance between opposite pyrrole nitrogens and the angles formed with the central Zn(II). [c] The distance between opposite meso−carbons and the angles formed with the central Zn(II). [d] The distance between the pyrrole nitrogens and the central carbon atoms on the outer perimeter of each fused acenaphthalene. [e] The angles formed with the opposite pyrolle nitrogen sitting on the same plane of symmetry.

(Figure 4). Michl[15] referred to cyclic polyenes in which the energy separation of the HOMOs (ΔHOMO) and the LUMOs (ΔLUMO) are both close to zero as soft MCD chromophores, since small structural perturbations that modify the OAM properties can reverse the alignment of the induced magnetic moments of the $\pi\pi^*$ excited states and hence the sign of Faraday $\mathscr{A}_1$ terms.

Results

(1) Optical Spectroscopy. The UV−visible absorption and MCD spectra of ZnTPTANP are reported in Figure 5, together with the key comparitive data[7] for the analogous TPP and octaethylporphyrin (OEP) complexes. Direct comparison of the spectral data for TPTANP with the simpler porphyrins is essential when analyzing the effect of steric hindrance on the spectral properties and electronic structure of the π−system. The data are plotted using a wavenumbers scale so that the energy separations between the major spectral bands of different complexes can be readily compared. In marked contrast with the spectra of ZnOEP and ZnTPP the MCD spectrum of ZnTPTANP contains negative Faraday $\mathscr{A}_1$ terms at 717 and 552 nm, and a positive $\mathscr{A}_1$ term at 666 nm, corresponding to the absorption maximum at 659 nm, Figure 5. Significantly, positive Faraday $\mathscr{A}_1$ terms are observed at 567, 698, and 759 nm in the case of $[H_4TPTANP]^{2+}$ and despite the marked red shift of the major bands, the UV−visible absorption and MCD spectra of $[H_4TPTANP]^{2+}$ are clearly very similar to those of $[H_4OEP]^{2+}$ and $[H_4TPP]^{2+}$. The sign sequence observed in the MCD spectrum of ZnTPTANP is highly unusual since positive $\mathscr{A}_1$ terms are usually the dominant feature within the MCD spectra of high symmetry metal porphyrinoids. Coupled oppositely signed Faraday $\mathscr{B}_0$ terms with *x*- and *y*-polarization are observed in the MCD spectra of H_2OEP, H_2TPP, and H_2-TPTANP as would be anticipated given the loss of the main 4-fold axis of symmetry, Figure 5.

We tabulate the major optical transitions predicted to the red of 300 nm (33 333 cm^{-1}) for ZnP, ZnTPP, ZnTANP, and ZnTPTANP by TD−DFT calculations in Table 2. The 1b → 1e* and 2b → 1e* one electrons transitions associated with the largest eigenvectors within the two lowest energy singlet excited states of ZnTPTANP correspond directly to the $1a_{2u} \rightarrow 1e_g^*$ and $1a_{1u} \rightarrow 1e_g^*$ which are the dominant contributions to the Q and B bands of ZnP within by Gouterman's 4−orbital and Michl's perimeter model. The energy separation of ca. 5000 cm^{-1} between the negative Faraday $\mathscr{A}_1$ terms of ZnTPTANP at 717 and 552 nm, Figure 5, is similar to the ca. 7000 cm^{-1} separation of the Q and B bands of ZnOEP and ZnTPP. TD−DFT calculations for ZnTPTANP, Table 2, predict only one, orbitally degenerate, electronic band to the blue of the main absorption band. Since no significant temperature dependence was observed in the UV−visible absorption spectra at room and cryogenic temperatures, and similar absorption and MCD spectra were obtained in a range of different solvents, a monomer dimer equilibrium is clearly not present. The negative

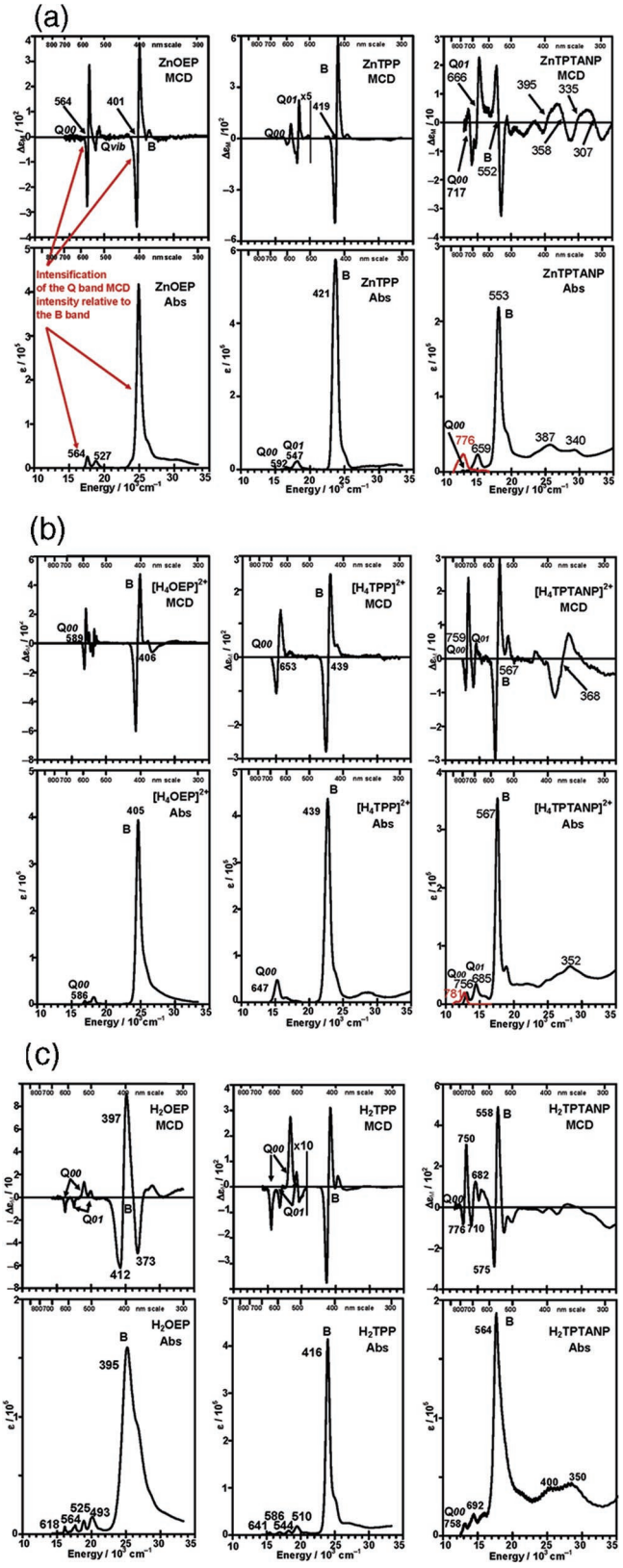

Figure 5. Absorption and MCD spectra of ZnTPP, ZnOEP, ZnTPTANP recorded in CH_2Cl_2, $[H_4OEP]^{2+}$, $[H_4TPP]^{2+}$, $[H_4TPTANP]^{2+}$, recorded in $CHCl_3$, H_2OEP and H_2TPP recorded in DMA and $H_2TPTANP$ recorded in THF at 298 K. Emission data for ZnTPTANP and $[H_4TPTANP]^{2+}$ based on excitation at 545 and 555 nm, respectively, are shown in red. $[H_4TPTANP]^{2+}$ was generated from ZnTPTANP with a trace of trifluoroacetic acid.

Faraday $\mathcal{A}_1$ terms can therefore be assigned as the Q_{00} and B_{00} bands, respectively, based on the allowed and forbidden nature of the corresponding absorption bands, while the positive $\mathcal{A}_1$ term at 666 nm can be assigned as a vibrational band (Q_{vib}). The very low Q band absorption intensities for ZnTPP and ZnTPTANP can be readily accounted for based on accidental near degeneracy of the HOMOs resulting in an almost fully forbidden Q band. Perrin[29] demonstrated that the Q band of soft MCD chromophores such as ZnOEP gain intensity from the allowed B band through a vibrational borrowing mechanism via a_{1g}, a_{2g}, b_{1g}, and b_{2g} modes and the Faraday $\mathcal{A}_1$ terms associated with the Q_{00}, Q_{01}, Q_{02} bands alternate in sign. The weaker bands at 340 and 387 nm can be assigned on the basis of the TD−DFT spectra of ZnP, ZnTPP, ZnTANP, ZnTPTANP, Table 2, to both *z*− and *x*/*y*-polarized transitions involving MOs introduced to the π−system by ligand expansion. Comparison of the Q and B band regions of the MCD spectra of ZnTPP and ZnTPTANP, Figure 5, suggests that the shoulder on the blue side of the B band is almost certainly vibrational rather than electronic in origin. It should be noted that the MCD data clearly identify the Q_{00} band at 717 nm, approximately 45 nm to the red of previous assignments by Lash,[10] who reported that the Q band lies at 672 nm. MCD and emission spectroscopy are often required to definitively identify the electronic origin of the forbidden Q transition within Gouterman's 4-orbital model, Figure 3.

The Faraday $\mathcal{A}_1$ terms observed at 763 and 568 nm in the MCD spectrum of $[H_4TPTANP]^{2+}$, Figure 5, can reasonably be assigned as the Q_{00} and B_{00} bands, respectively, while the $\mathcal{A}_1$ term at 698 nm can be assigned as a Q_{vib} band. The Q band region of $[H_4TPP]^{2+}$ and $[H_4TPTANP]^{2+}$ contains a much less complex set of vibrational bands than that of $[H_4OEP]^{2+}$ due to the lack of peripheral substituents. The Q_{00} absorption band of $[H_4TPTANP]^{2+}$ is significantly more intense than the Q_{00} band of ZnTPTANP at 717 nm and the Q_{00} emission band shows mirror symmetry with the main Q band region absorption band, Figure 5. A similar intensification of the Q_{00} absorption band can be observed in the spectrum of $[H_4TPP]^{2+}$, while in contrast the Q_{00} band of $[H_4OEP]^{2+}$ is almost completely forbidden. Recent variable temperature NMR studies of TPP complexes[6c,30] and TD−DFT[31] calculations have invoked a saddled structure to account for a reduced energy barrier for rotation of the phenyl substituents of dication species relative to the planar Zn(II) complex. Saddled geometries were reported for $[H_4TPP]^{2+}$ and $[H_4OEP]^{2+}$ in the late 1960s by Stone and Fleischer based on X-ray crystallography structures.[32] In the case of $H_2TPTANP$ in THF, weak Q_{00} bands at 776 and 750 nm and Q_{01} band at 710 and 682 nm lie to the red of the main absorption band center arising from the B transition at 564 nm. The negative $\mathcal{B}_0$ terms of the symmetry split Q_{00} and Q_{01} bands lie at lower energy as is the case with H_2TPP and H_2OEP, but the energy separations between the Q*x* and Q*y* bands are significantly smaller so the typical free base porphyrin pattern of two negative $\mathcal{B}_0$ terms followed by two positive $\mathcal{B}_0$ terms is no longer observed, Figure 6.

(29) Perrin, M. H. *J Chem. Phys.* **1973**, *59*, 2090−2104.
(30) Freitag, R. A.; Whitten, D. G *J. Phys. Chem.* **1983**, *87*, 3918−3925.
(31) Ricciardi, G.; Rosa, A.; Baerends, E. J.; Romeo, A.; Scolaro, L. M. *J. Phys. Chem. A* **2003**, *107*, 11468−11482.
(32) Stone, A.; Fleischer, E. B. *J. Am. Chem. Soc.* **1968**, *90*, 2735−2748.

Table 2. Calculated Electronic Excitation Spectra of ZnP, ZnTPP, ZnTANP, ZnPc and ZnTPTANP Based on TD−DFT with 6−31G(d) Basis Sets, Figure 9[g]

band[a]	no.[b]	sym.[c]	calcd.[d]	exp[e]	wave function[f]=
			ZnP (D_{4h})		
Q	**2,3**	^1E_u	19.7 (0.00)	17.5	**.46|1e$_{gy}$*←1a$_{1u}$>+0.46|1e$_{gx}$*←1a$_{2u}$>+.23|1e$_{gx}$*←1a$_{1u}$>−.23|1e$_{gx}$*←1a$_{2u}$>+..**
B	**6,7**	^1E_u	28.6 (0.90)	24.9	**.35|1e$_{gx}$*←1a$_{1u}$>+.34|1e$_{gx}$*←1a$_{2u}$>−.16|1e$_{gx}$*←1a$_{1u}$>+.15|1e$_{gy}$*←1a$_{2u}$>+..**
	10,11	^1E_u	31.0 (0.05)		+.67|1e$_{gy}$*←1b$_{1u}$>+....
			ZnTPP (C_4)		
Q	**2,3**	^1E	18.7 (0.01)	17.1	**.51|1e$_y$*←1a>−.46|1e$_x$*←1a>+....**
B	**4,5**	^1E	26.8 (0.73)	24.0	.42|1e$_y$*←1b^N>**−.32|1e$_x$*←2a>−.25|1e$_y$*←1a>**.17|1e$_x$*←1b^N>+....
	6,7	^1E	26.9 (0.62)		.53|1e$_y$*←1b^N>+**.26|1e$_x$*←2a>+.22|1e$_y$*←1a>+....**
			ZnTANP (D_{4h})		
Q	**2,3**	^1E_u	15.9 (0.13)	−[g]	**.54|1e$_{gy}$*←1a$_{1u}$>+0.44|1e$_{gx}$*←1a$_{2u}$>+...**
B	**4,5**	^1E_u	20.0 (0.95)	−[g]	**.47|1e$_{gy}$*←1a$_{2u}$>+0.34|1e$_{gx}$*←1a$_{1u}$>+....**
	26,27	^1E_u	26.4 (0.17)		.67|1e$_{gy}$*←2b$_{1u}$>+.17|2e$_{gx}$*←1a$_{1u}$>+....
	30,31	^1E_u	27.8 (0.13)		.55|2e$_{gy}$*←1a$_{1u}$>+.38|2e$_{gx}$*←1a$_{2u}$>+....
	32,33	^1E_u	28.7 (0.17)		.53|1e$_{gy}$*←2a$_{1u}$>−.33|2e$_{gx}$*←1a$_{2u}$>−.20|1b$_{2u}$*←2e$_{gx}$>+....
			ZnPc (D_{4h})		
Q	**2,3**	^1E_u	16.6 (0.41)	14.8	**.60|1e$_{gy}$*←1a$_{1u}$>−0.23|1e$_{gx}$*←1a$_{2u}$>+...**
B1	**17,18**	^1E_u	29.3 (0.17)	29.9	.48|1e$_{gy}$*←2a$_{2u}$>**+0.45|1e$_{gy}$*←1a$_{2u}$>**+.16|1e$_{gx}$*←1b$_{2u}$>+...
B2	**19,20**	^1E_u	30.0 (0.36)		.63|1e$_{gy}$*←1b$_{2u}$>**−0.22|1e$_{gx}$*←1a$_{2u}$>**+.17|2e$_{gy}$*←1a$_{1u}$>+...
	25,26	^1E_u	30.8 (0.32)		.43|1e$_{gy}$*←2a$_{2u}$>**−0.38|1e$_{gy}$*←1a$_{2u}$>**−.24|1e$_{gx}$*←2a$_{1u}$>−.20|1e$_{gx}$*←1b$_{2u}$>+...
			ZnTPTANP (S_4)		
Q	**2,3**	^1E	14.4 (0.00)	13.1	**.51|1e$_y$*←1b>−.44|1e$_x$*←2b>−.16|1e$_x$*←1b>+.13|1e$_y$*←2b>+....**
B	**4,5**	^1E	18.3 (0.90)	17.6	**.45|1e$_y$*←2b>+.34|1e$_x$*←1b>+....**
	11	^1B	20.3 (0.10)		.57|1a*←2b>+.27|1e$_y$*←1e$_x$>−.27|1e$_x$*←1e$_y$>+....
	12	^1B	20.9 (0.09)		.42|1e$_y$*←1e$_x$>−.40|1e$_x$*←1e$_y$>−.37|1a*←2b>+....
	14,15	^1E	21.9 (0.04)		.65|1e$_y$*←3b>+.19|1e$_x$*←1a>+....
	19	^1B	23.8 (0.24)		.53|1e$_x$*←2e$_x$>+.41|1e$_y$*←2e$_y$>+....
	21,22	^1E	24.5 (0.06)		.68|1e$_y$*←2a>+....
	29,30	^1E	26.2 (0.28)		.59|2e$_y$*←1b>−.24|1e$_x$*←5b>+.21|2e$_x$*←2b>+....
	35,36	^1E	28.1 (0.05)		.54|1e$_y$*←3a>−.19|1e$_x$*←3e$_x$>+....

[a] Band assignment described in the text. [b] The number of the state assigned in terms of ascending energy within the TD−DFT calculation. Only states located below 30, 000 cm^{-1} (except for ZnPc) resulting from allowed electronic transitions with an oscillator strength of greater than 0.05 are included.[c] The state symmetry. [d] Calculated band energies (10^3.cm^{-1}) and oscillator strength. [e] Observed energies (10^3.cm^{-1}), Table 5. [f] The wave functions based on the eigenvectors predicted by TD−DFT. One-electron transitions associated with Gouterman's 4-orbital model, Figure 3, are shown in bold. Only eignenvectors greater than 0.15 are included. **f** − No data available. [g] Calculated spectra obtained with 6−31G basis sets and by using INDO/s on the CAChe workstation are shown in Table S2. A correlation table enables comparison of MOs of different symmetry, Table 3.

Table 3. Correlation Table for MOs with D_{4h}, D_{2d}, C_4, and S_4 Symmetry[a]

D_{4h}	D_{2d}	C_4	S_4	D_{4h}	D_{2d}	C_4	S_4	D_{4h}	D_{2d}	C_4	S_4
a_{1u}	b_1	a	b	b_{1u}	a_2	b	a	e_g	e	e	e
a_{2u}	b_2	a	b	b_{2u}	a_1	b	a				

[a] MO labels and energies are also correlated and tabulated in Table S3 based on the distinctive π-MO nodal patterns.

(2) Spectral Band Deconvolution and Excited-State Magnetic Moments. Spectral band deconvolution analyses of ZnTPTANP and [H$_4$TPTANP]$^{2+}$ based on the SIMPFIT program[8,12,33−35] are shown in Figure 6. Simultaneous spectral band deconvolution of MCD and absorption spectra removes much of the ambiguity that is normally associated with band deconvolution analyses. Under the Rigid Shift Assumption,[26] the application of a magnetic field does not alter the Gaussian-shaped band curve function within the MCD intensity mechanism so the same bands widths and centers are used to fit both spectra. A slight deviation from the ideal first-derivative of the Gaussian band shape for the $\mathscr{A}_1$ terms in the case of [H$_4$-TPTANP]$^{2+}$ points to a minor zero-field splitting of the $\pi\pi^*$ excited states. Excited-state magnetic moments were derived from the deconvoluted bands, Figure 6, using Stephens, Piepho, and Schatz's[25a,b] modified conventions for $\mathscr{A}_1$, $\mathscr{B}_0$, and $\mathscr{D}_0$ for randomly oriented molecules which differ substantially from an older set of conventions used by other authors such as Briat[27] and Michl.[15] The $\mathscr{A}_1/\mathscr{D}_0$ ratios of the Q_{00} and B_{00} bands of ZnTPTANP (−2.2 β and −0.2 β, respectively) and [H$_4$-TPTANP]$^{2+}$ (1.1 β and 0.2 β, respectively), are somewhat lower in magnitude than values obtained for ZnOEP (4.3 β and 0.8 β, respectively). Ceulemans et al. obtained an $\mathscr{A}_1/\mathscr{D}_0$ ratio of 4.39 β for ZnOEP using a similar spectral band deconvolution analysis in benzene.[36] It should be noted that positive magnetic moments result in negative $\mathscr{A}_1$ terms due a difference in the perspective used to define handedness within magnetism and classical optics. Method of moments magnetic moment calculations similar to those we have reported previously for the Q band region of phthalocyanines[35c] would be challenging in the case of TPTANP due to the lack of baseline to baseline band envelopes.

(2) Molecular Modeling. By carrying out calculations over the wide range of compounds shown in Figure 2 we can assemble series of comparable data that identify consistencies in the calculations and underlying electronic control of the observable spectral parameters, namely, band energies, band

(33) (a) Browett, W. R.; Stillman, M. J. *Inorg. Chim. Acta* **1981**, *49*, 69−77. (b) Gasyna, Z.; Browett, W. R.; Nyokong, T.; Kitchenham, R.; Stillman, M. J. *Chemom. Intell. Lab. Syst.* **1989**, *5*, 233−246. (c) Mack, J. *Ph.D. Thesis*, University of Western Ontario 1994.
(34) Mack, J.; Stillman, M. J. *J. Phys. Chem.* **1995**, *99*, 7935−7945.
(35) (a) Nyokong, T.; Gasyna, Z.; Stillman, M. J. *Inorg. Chem.* **1987**, *26*, 548−553. (b) Nyokong, T.; Gasyna, Z.; Stillman, M. J. *Inorg. Chem.* **1987**, *26*, 1087−1095. (c) Ough, E. A.; Nyokong, T.; Creber, K. A. M.; Stillman, M. J. *Inorg. Chem.* **1988**, *27*, 2724−2732. (d) Mack, J.; Stillman, M. J. *Inorg. Chem.* **1997**, *36*, 413−425.
(36) (a) Ceulemans, A.; Oldenhof, W.; Görller-Walrand, C.; Vanquickenborne, L. G. *J. Am. Chem. Soc.* **1986**, *108*, 1155−1163.

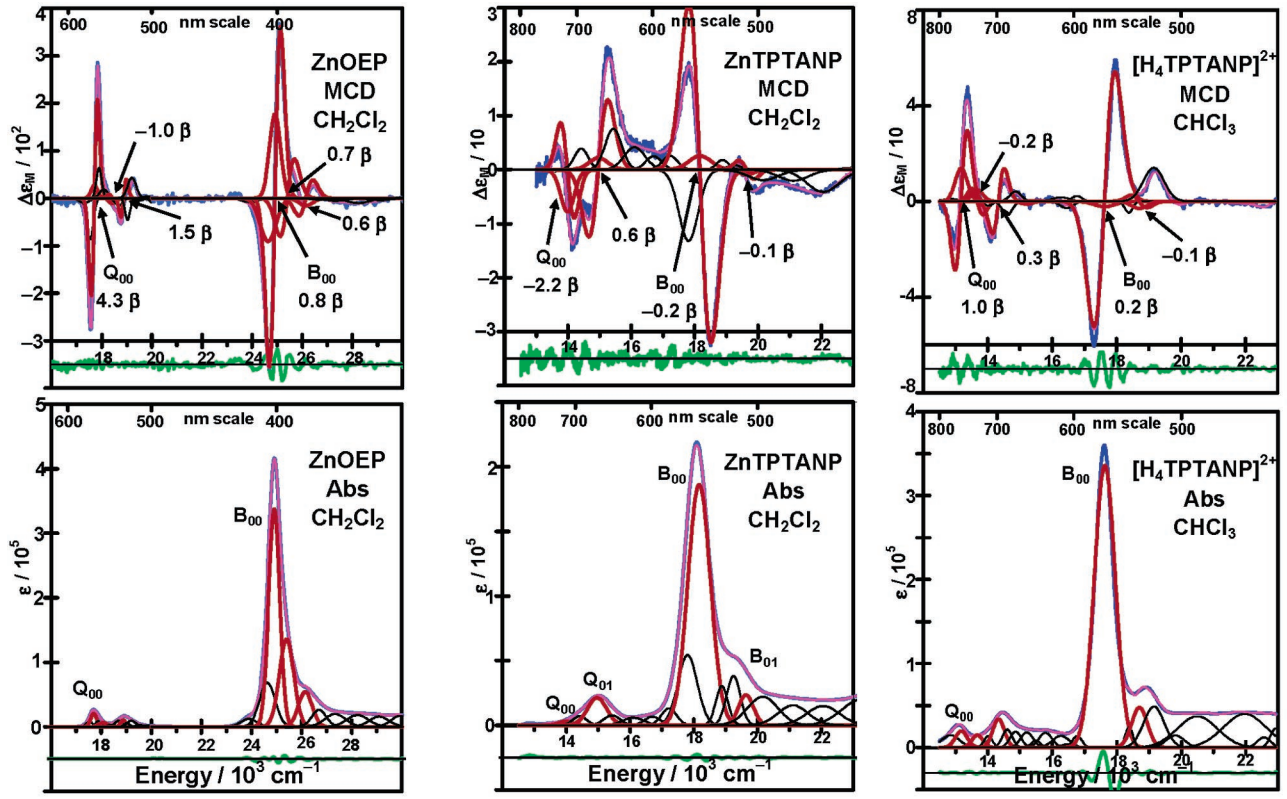

Figure 6. Spectral deconvolution analyses of the absorption and MCD spectra of ZnOEP and ZnTPTANP recorded in CH_2Cl_2 and $[H_4TPTANP]^{2+}$ recorded in $CHCl_3$ at 298 K and the $\mathscr{A}_1/\mathscr{D}_0$ ratios associated with the $\mathscr{A}_1$ terms. Purple, blue, green, black, and red lines represent the calculated spectrum, the residual of the calculated fit, the experimentally observed spectral data, the component deconvoluted bands and bands associated with MCD $\mathscr{A}_1$ terms, respectively. The band parameters are available in Table S4.

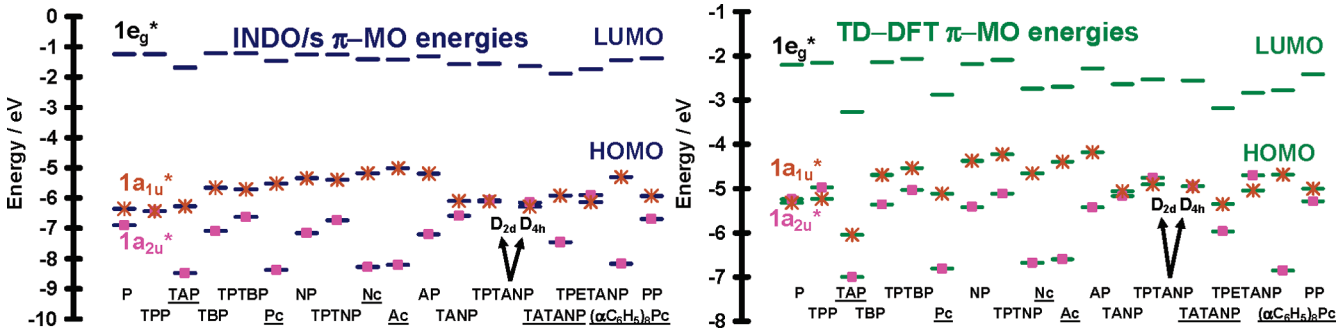

Figure 7. Trends in the energies of the 4 frontier π-MOs from Gouterman's model from INDO/s, (middle) and TD-DFT calculations (bottom) based on optimizations with 6−31G basis sets. The MO energies and symmetries are tabulated in Table S6. Aza-substituted-porphyrinoids are underlined.

intensities and polarization and magnetic moment values. We present the results of these calculations in a series of detailed figures that show (i) the calculated energies of the 4 frontier π-MOs, comparing the results from the DFT and INDO approaches (Figure 7), (ii) show trends in the oscillator strengths and induced excited-state magnetic moments of the Q and B/B1 bands as a function of ΔHOMO (Figure 8 and Table 4), (iii) the calculated spectral data, comparing results from INDO/s and TD−DFT calculations (Figure 9), (iv) comparison between the observed and the calculated energies of the Q and B/B1 bands (Figure 10 and Table 5), and finally, (vi) the calculated percentage contribution of the one electron transitions associated with Gouterman's 4-orbital to the Q and B/B1 bands, Table 6.

Major structural perturbations such as the addition of fused benzene rings and/or aza−nitrogens break the accidental near-degeneracy of the $1a_{1u}$ and $1a_{2u}$ HOMOs significantly, Figure 7, resulting in hard MCD chromophores with large magnetic moments associated with the B excited state that cannot easily be reversed by minor structural modifications, Figure 8 and Table 4. Both TD−DFT and INDO/s calculations predict that when structural perturbations break the near degeneracy of the $1a_{1u}$ and $1a_{2u}$ HOMOs of ZnP, thus introducing a significant increase in ΔHOMO, the Q band gains intensity, since the Q and B bands lose their ideal forbidden and allowed characters. Despite the saddled S_4 symmetry structure, ZnTPTANP has one of the smallest predicted ΔHOMOs for the range of porphyrinoids shown in Figure 2. The four one−electron transitions associated with Gouterman's 4−orbital model[7] are consistently responsible for the lowest energy $\pi \rightarrow \pi^*$ band and the most intense band within the calculated porphyrinoid UV−visible absorption spectra derived from both the TD−DFT and INDO/s techniques, Figure 9 and Table 6.

In the case of soft MCD chromophores, such as ZnP, ZnTPP and ZnTPTANP, Table 2, the $1a_{1u} \rightarrow 1e_g$ and $1a_{2u} \rightarrow 1e_g$

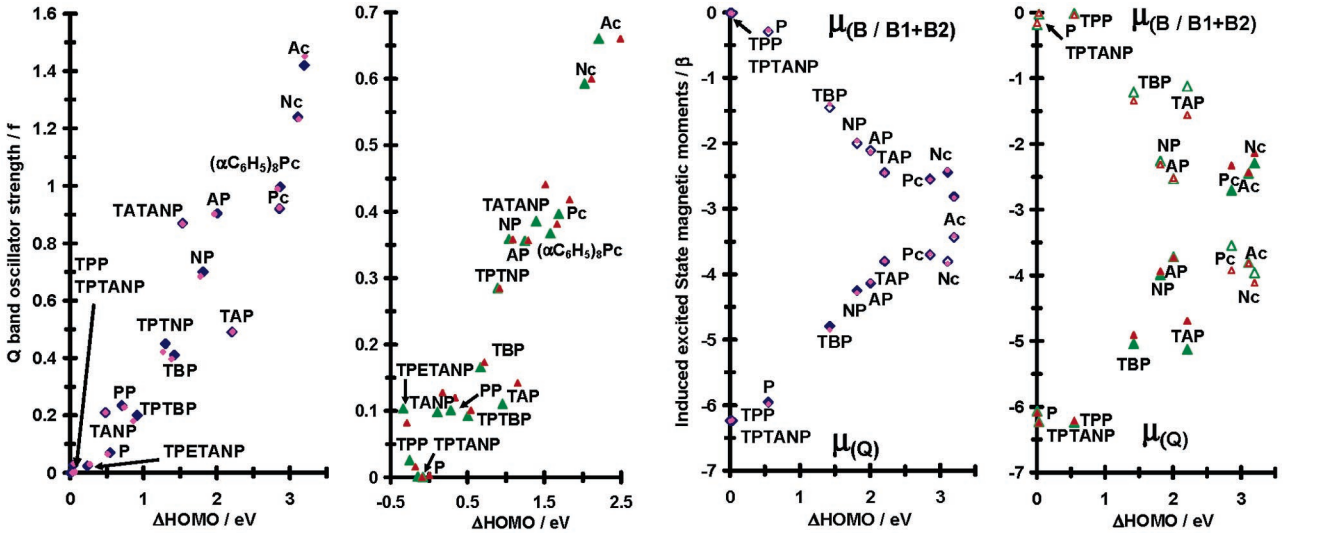

Figure 8. The calculated Q band oscillator strengths from INDO/s (left) and TD−DFT (center left) calculations based on 6−31G and 6−31G(d) basis sets plotted against ΔHOMO. Calculated excited-state magnetic moments derived from the oscillator strengths of the Q and B/B1 bands within the INDO/s (RIGHT) and TD−DFT (CENTER RIGHT) calculations based on eq 1.[15a,36a] 6−31G data are plotted with blue diamonds and green triangles, while 6−31G data are plotted with magenta diamonds and red triangles, respectively. Open symbols refer to μ(B), while filled symbols refer to μ(Q). In the case of the hard MCD chromophores, the oscillator strengths of the B1 and B2 bands, Figure 9 and Table S5 are combined within the calculation of α, Table 4.

Table 4. Calculated and Observed Excited State Magnetic Moments

	α[a]	μ(Q) (TD)[a]	μ(B)	α[a]	μ(Q) (I)[a]	μ(B)	μ(Q)[b] EXP	no.[c]	α	μ(Q)	μ(B) (TD)[a]	α	μ(Q)	μ(B) (I)[a]	μ(B)	μ(Q)[b] EXP	no.[c]
P	1.2°	−6.2	0.0	9.3°	−6.08	−0.17	−4.3		**Nc**	38.8°	−2.5	−3.8	35.9°	−2.15	−4.10	−2.9[d]	**49**
TAP	21.3°	−5.4	−0.8	31.1°	−4.58	−1.67	−4.8[d]	**49**	**NP**	29.4°	−1.5	−4.7	24.7°	−1.10	−5.15		
TBP	21.4°	−5.4	−0.8	21.0°	−5.44	−0.81			**Ac**	39.0°	−2.5	−3.8	36.7°	−2.24	−4.01	−1.2[d]	**49**
Pc	39.1°	−3.8	−2.5	38.7°	−3.81	−2.44	−1.3		**AP**	30.6°	−1.6	−4.6	29.8°	−1.55	−4.70		
TPP	8.0°	−6.1	−0.1	0.3°	−6.24	−0.01	−2.5	**36a**	**TPTANP**	2.2°	0.0	−6.2	2.4°	−0.02	−6.23	2.2	

[a] α, μ(Q), μ(B) are calculated on the basis of eq 1, Figure 8. [b] Experimental (EXP) μ(Q) values. [c] References for **b**. [d] Data for Co^{II} complexes calculated according to methods developed by Briat et al.[27]

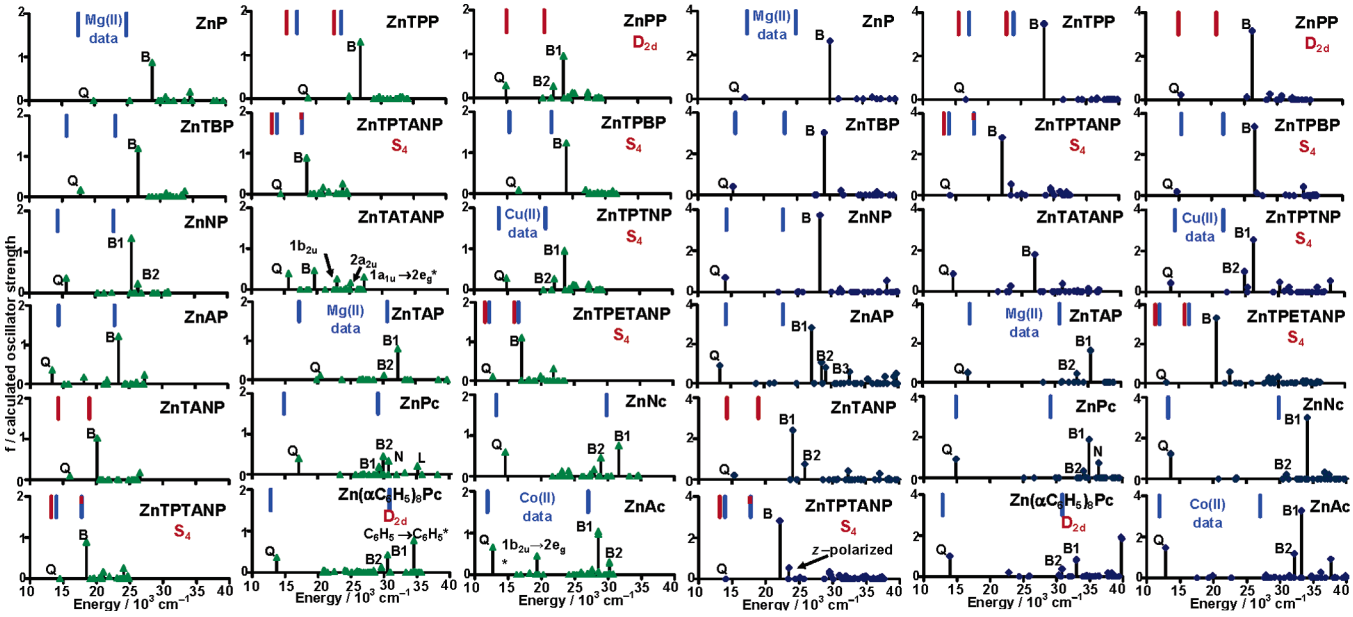

Figure 9. Calculated spectra generated from the TD−DFT (LEFT) and INDO/s (RIGHT) calculations for the complexes in Figure 2 using Gaussian 03.[31] The band centers are indicated with green triangles and blue diamonds, respectively. Band parameters for the allowed x/y-polarized transitions of ZnP, ZnTPP, ZnTANP, ZnTPTANP, and ZnPc are shown in Table 2. Vertical blue lines indicate the energies of the Q and B bands observed experimentally, Table 5, while red lines denote the energy of the Q and B bands of dication species reported by Lash.[10] The B1/B2 band terminology, developed for the multiple intense Faraday $\mathcal{A}_1$ terms in the UV region of MPc,[8,12,35] Table 2, is applied in the case of hard MCD chromophores. Calculated spectra obtained for 6−31G(d) structures are available in Figure S2.

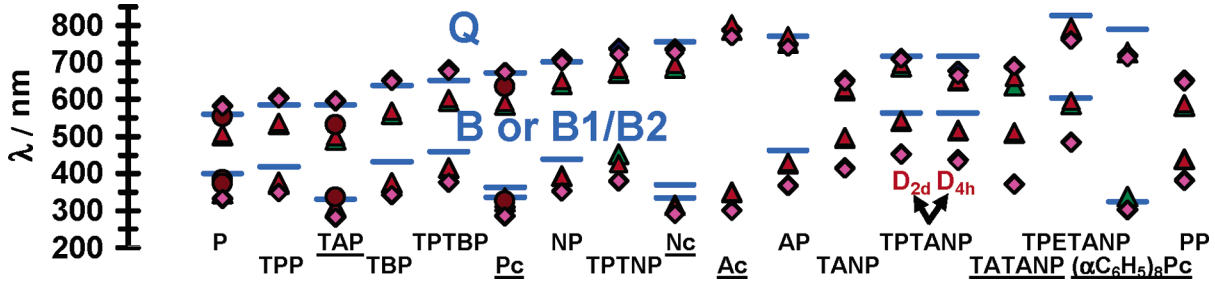

Figure 10. Calculated (symbols) and observed (lines) wavelengths of the Q and B/B1 transitions of the Zn(II) complexes of the porphyrinoid ligands in Figure 2. Data obtained from INDO/s and TD−DFT based on B3LYP DFT geometry optimizations with 6−31G and 6−31G(d) basis sets appear as blue and magenta diamonds and green and red triangles, respectively. Data reported by Baerends et al. based on SAOP and the Amsterdam Density Functional package appear as brown circles.[28k] The calculated wavelengths and intensities and observed experimental values are tabulated in Table 5. Calculated spectra based on the 6−31G basis sets optimizations are plotted in Figure 8.

Table 5. Q and B/B1 Band Wavelengths Band Intensities (ϵ) and Calculated Oscillator Strengths

	Q λ_{max} [a]/nm			B/B1 λ_{max} [b]/nm			$10^3.\epsilon_{max}$ [c,h]		Q[d](f)		B/B1[e](f)		no.[f]
	Ex	IN	TD	Ex	IN	TD	Q	B[1]	IN	TD	IN	TD	
P	572	583	503	402	333	348	5.4 **[Mg]**	487 **[Mg]**	0.07	0.00	2.64	0.88	40
TAP	584	596	491	326	283	310	107 **[Mg]**	62 **[Mg]**	0.49	0.11	1.62	0.79	41
TPP	586	604	533	419	351	372	3.5	574	0.00	0.03	3.47	1.30	42
TBP	638	652	561	432	343	375	130	400	0.41	0.17	3.02	1.18	43
Pc	672	673	585	343	286	334	282	71	0.92	0.40	1.88	0.45	44
TPTBP	651	680	595	459	377	416	60	230	0.20	0.09	3.35	1.24	17
NP	701	708	642	439	353	393	66	46.8	0.70	0.36	3.72	1.33	45
TPTNP	710	728	672	470	381	422	115 **[Cu]**	120 **[Cu]**	0.45	0.28	2.54	0.96	46
Nc	756	735	685	335	293	315	390	110	1.24	0.59	3.00	0.75	47
AP	771	749	753	463	369	428	180	160	0.90	0.36	2.82	1.22	48
Ac	839	779	787	370	301	350	700 **[Co]**	480 **[Co]**	1.46	0.66	3.26	1.04	49
TANP		652	624		415	497			0.21	0.10	2.41	1.02	
TPTANP	717	711	689	563	452	541	3.9	219	0.00	0.00	2.80	0.89	
TPTANP		665	651		432	516			0.00	0.02	3.4	1.09	
(D_{4h})[g]		46	38		20	25			saddling red shift (nm)[g]				
TATANP		688	639		371	510			0.87	0.39	1.81	0.46	
TPETANP	826	762	791	604	484	587	16	316	0.02	0.10	3.31	1.10	10
PP		652	582	–	382	439			0.23	0.10	3.15	0.55	
($\alpha C_6H_6)_8$Pc	780	718	727	324	303	338	800	600	1.00	0.37	0.82	0.13	18

[a,b] The experimental (EXP) and calculated wavelengths predicted by INDO/s (IN) and TD-DFT (TD) based on the geometry optimizations with 6-31G basis sets. [c] Extinction coefficients. [d,e] The calculated oscillator strengths predicted by INDO/s (IN) and TD-DFT (TD). [f] references for data in **c**. [g] A D_{4h} model geometry. [h] Data are for Zn(II) complexes unless otherwise specified.

Table 6. Per Centage Contribution of the Transitions from Gouterman's 4-orbital Model to the Q and B/B1 Bands Based on Eigenvector Values from INDO/s Calculations of the B3LYP Based Geometry Optimizations with 6−31G Basis Sets

	Q[a]	B/B1[a]	α[b]		Q[a]	B/B1[a]	α[b]		Q[a]	B/B1[a]	α[b]		Q[a]	B/B1[a]	α[b]
$C_{16}H_{16}^{2-}$	49:49	49:49	0°	**Pc**	91:6	22:55	50°	**AP**	85:9	4:45	36°	**TATANP**	86:8	5:46	49°
P	63:34	33:60	12°	**TPTBP**	70:27	26:67	19°	**Ac**	92:2	2:25	48°	**TPETANP**	52:42	41:51	6.1°
TAP	85:12	8:64	39°	**NP**	83:13	9:68	34°	**TANP**	65:28	23:52	18°	**PP**	71:23	22:59	20°
TPP	51:46	45:49	0.4°	**TPTNP**	78:18	39:42	28°	**TPTANP**	55:40	37:51	0.4°	**($\alpha C_6H_6)_8$Pc**	92:5	4:45	60°
TBP	78:19	19:72	29°	**Nc**	95:3	2:47	51°	**TPTANP (D_{4h})[c]**	44:49	47:43	3.0°				

[a] The percentage contribution of the $1a_{1u} \rightarrow 1e_g^*$ and $1a_{2u} \rightarrow 1e_g^*$ eigenvectors to the Q and B/B1, Table S5. [b] α the degree of mixing of the magnetic properties of the Q and B/B1 excited states on the basis of eq 1, Figure 8. [c] A D_{4h} model geometry.

contributions to the Q and B bands are almost identical in magnitude, Table 6, resulting in ideal forbidden and allowed bands, while for hard MCD chromophores such as ZnPc, the $1a_{1u} \rightarrow 1e_g$ one−electron transition becomes the dominant contribution to the Q band and substantial configurational interaction occurs within the B band region between the $1a_{2u} \rightarrow 1e_g$ one-electron transition and transitions involving π−MOs with similar energies to the $1a_{2u}^*$ MO from Gouterman's 4-orbital model, Figures 7−10.

Although TD−DFT calculations based on the B3LYP functional provide a more accurate estimate of the wavelengths of the B/B1 band, Figures 9 and 10, the semiempirical INDO/s calculations provide a better estimate of the wavelength of the Q band.

Discussion

(a) MCD Spectroscopy of TPTANP. The MCD spectra of ZnTPTANP and $[H_4TPTANP]^{2+}$, Figures 5 and 6, provide a classic example of how structural changes to a soft MCD chromophore can alter the magnetic properties of the hetero-aromatic π−system much more significantly than the electric-dipole-based UV−visible absorption spectrum. The MCD intensity mechanism is much more sensitive to saddling of the ligand's *xy*-plane than the electric dipole properties, which are based on linear translation of charge along the *x*-, *y*-, *or z*-axis, since the magnetic moments, Figure 11, are induced by the circular redistribution of charge on the inner perimeter of the π−system. Although the absorption intensity of the B band of

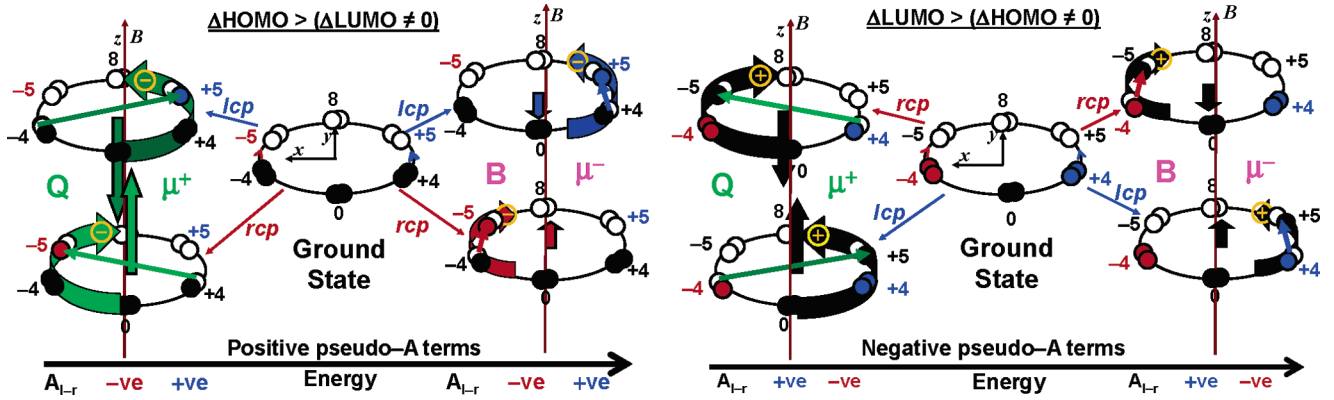

Figure 11. Application of Michl's perimeter model to the four spin allowed transitions within Gouterman's 4-orbital model, Figure 3. Pairs of colored circles are used to illustrate the occupancy of the four frontier π−MOs within each electronic state. Black signifies MOs in which the OAM properties on the inner perimeter are largely quenched due to a large ΔHOMO or ΔLUMO, while blue and red signify MOs with left and right-handed charge circulation. The small colored arrows correspond to the linear charge displacement associated with the four one-electron transition, while the curved larger arrows denote the resulting charge circulation on the inner ligand perimeter within each excited state after absorption of a photon of either lcp or rcp. Large curved black arrows signify circulation of a positively charged particle in instances where ΔLUMO > ΔHOMO, while colored arrows signify a negatively circulating charge in instances where ΔHOMO > ΔLUMO. The alignment of the induced magnetic moments are shown relative to the applied field based on the right-hand rule for conventional current flow. Microstates in which the dipole is aligned with the applied field are stabilized. The MCD sign is based on the CD convention of ΔA_{l-r}.

ZnTPTANP is of the same order of magnitude as the B bands of planar porphyrinoid complexes, Table 5, the MCD signal is over an order of magnitude weaker than that of ZnOEP and ZnTPP, Figure 5, probably as a result of an increase in Faraday $\mathscr{B}_0$ term intensity. Michl[15] accounted for the MCD sign sequences observed for the Q and B bands within aromatic and heteroaromatic cyclic polyenes, based on the mixing of the induced excited-state magnetic moments (μ^+ and μ^-), Figure 11. Michl[15a] predicted, based on LCAO calculations, that μ^+ and μ^- of a $C_{16}H_{16}^{2-}$ cyclic polyene perimeter are $-0.01\ \beta$ and $-6.24\ \beta$, respectively. For an ideal D_{16h} perimeter with ΔLUMO, ΔHOMO = 0, the Q_{00} band is fully electric dipole forbidden and can gain intensity only through vibrational borrowing from the allowed B_{00} band and hence the MCD sign of the B_{00} band is determined by μ^-. In reduced symmetry, planar D_{4h} cyclic perimeters, where ΔHOMO ≠ 0, ΔLUMO = 0, there is a mixing of the allowed and forbidden character of the Q and B transitions and the Q and B bands can acquire both μ^- and μ^+ character, Figure 8. Estimates for the degree of mixing of the magnetic properties, α, and the magnitude of the induced magnetic dipole moments of the Q and B excited states (μ(Q), μ(B)) can be calculated using eq 1, which was originally derived within Michl's perimeter model,[15a,36] by converting the calculated oscillator strengths derived from INDO/s and TD−DFT calculations into dipole strengths based on Stephens, Piepho and Schatz's[25a,b] modified convention for $\mathscr{D}_0$, Figure 8 and Table 4.

$$\mathscr{D}_0(\mathrm{Q})/\mathscr{D}_0(\mathrm{B}) = \tan^2\alpha \quad \mu(\mathrm{B}) = \pm(\cos^2\alpha)\mu^- \pm(\sin^2\alpha)\mu^+$$
$$\mu(\mathrm{Q}) = \pm(\sin^2\alpha)\mu^- \pm(\cos^2\alpha)\mu^+ \quad (1)$$

The positive Faraday $\mathscr{A}_1$ terms that would be anticipated on the basis of the negative μ(Q) values have been observed consistently for planar metal porphyrinoids with a 4-fold axis of symmetry, Figure 8, and also for saddled hard MCD chromophores such as ZnTPTBP[17] and $Zn(\alpha C_6H_5)_8Pc$,[18] since the OAM associated with the orbitally degenerate LUMO is greater than that associated with the HOMOs due to the large ΔHOMO. The highly unusual negative Faraday $\mathscr{A}_1$ terms observed for the Q and B bands of ZnTPTANP, therefore, represent direct spectroscopic evidence for folding of the ligand, which could not be obtained from either ^{1}H NMR or UV−visible absorption spectroscopy. Michl[15b] demonstrated that the alignment of the magnetic moments and the ordering of the MCD signs for the Q*y*, Q*x*, B*y*, B*x* bands of soft MCD chromophores could be determined by the relative magnitude of ΔHOMO and ΔLUMO. When ΔHOMO > ΔLUMO, the ordering of the MCD intensity signs for the Faraday $\mathscr{B}_0$ terms associated with the Q and B bands is −ve, +ve, −ve, +ve in ascending energy (analogous to two positive $\mathscr{A}_1$ terms), Figure 11. In contrast, when ΔLUMO > ΔHOMO the sequence reverses to the +ve, −ve, +ve, −ve (analogous to two negative $\mathscr{A}_1$ terms), the situation observed in the MCD spectra of the chlorins since ΔLUMO > ΔHOMO due to the effect of the reduction of the porphyrin π−system at the ligand periphery. In the case of the chlorins, a positive particle (associated with the hole within the HOMO) is effectively formed on the cyclic perimeter, due to the imbalance caused when OAM associated with the electron within the LUMO within the excited state is no longer fully compensated by a second electron within an MO of the opposing handedness. The effect observed for ZnTPTANP is not directly analogous to the sign reversal of chlorins and bacteriochlorins, however, since derivative-shaped Faraday $\mathscr{A}_1$ terms are observed rather than coupled oppositely signed Gaussian-shaped $\mathscr{B}_0$ terms which are associated with a lifting of the orbital degeneracies of the excited states.[19] The MCD sign reversal must, therefore, be the result of a structural perturbation that is symmetric with respect to the 4-fold axis of symmetry of the $C_{16}H_{16}^{2-}$ parent cyclic perimeter and that disrupts the OAM properties of the LUMO to a greater extent than those of the HOMO. The forbidden nature of the Q_{00} absorption band of ZnTPTANP, Figure 5, and the negative Faraday $\mathscr{A}_1$ terms identified by spectral band deconvolution in Figure 6, are direct spectroscopic evidence that TPTANP is a double-soft MCD chromophore with ΔHOMO, ΔLUMO ≈ 0. Further support for this interpretation is provided by TD−DFT calculations based on 6−31G(d) basis sets, which predict an

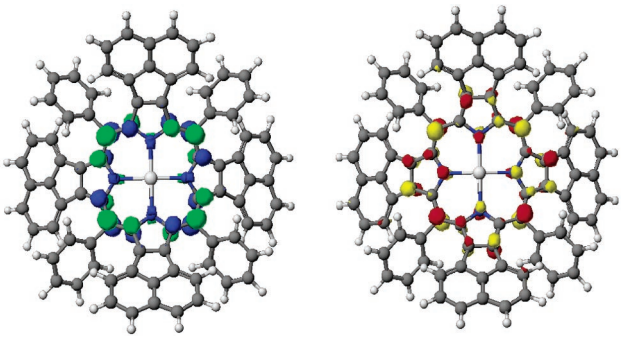

Figure 12. HOMOs (LEFT) and LUMOs (RIGHT) of ZnTPTANP predicted by the CAChe workstation tabulator program at an isosurface value of 0.06 au.

oscillator strength of 0.0000 for the Q band of ZnTPTANP. Although the μ^+ properties should therefore be fully electronically forbidden (based on $\alpha = 0°$) resulting in a sign sequence of 0, 0, −ve, +ve, the μ^- moment associated with the $C_{16}H_{16}^{2-}$ parent perimeter is small enough that minor structural modifications can alter the MCD sign sequences for the Q and B bands. We see in Figure 12 based on an INDO/s calculation from the B3LYP geometry, that the contours of the 1e LUMO of ZnTPTANP at an isosurface value of 0.06 au extend out toward the periphery of the ligand, while those of the accidentally degenerate $1b_1$ and $1b_2$ HOMOs are confined primarily to the inner perimeter. The deep "frozen saddle" geometry first proposed by Lash,[10] which is predicted by B3LYP calculations, Figure 1 and Table 1, therefore perturbs the OAM properties of the LUMO sufficiently to enable a complete reversal of the MCD sign sequence based on a vibronic intensity borrowing mechanism.

Anomalous MCD sign sequences have previously been observed only rarely in the case of metal porphyrinoids with symmetric perimeters. A +ve, −ve, −ve, +ve sign sequence was reported by Djerassi and co-workers,[37] in the case of double-soft chromophores such as tetrakis(pentafluorophenyl)porphyrin and for a series of tetrakis(*ortho*−halophenyl)porphyrins. A variety of possible electronic and vibronic based explanations have been proposed[36] with Ceulemans[37] concluding that substituent effects resulted in a $C_{16}H_{16}^{2-}$ based soft MCD chromophore with ΔHOMO, ΔLUMO $\approx$ 0 and that a specific vibronic intensity mechanism that was not part of either Gouterman's 4-orbital or Michl's perimeter model was responsible for the observed MCD sign sequence reversals. Although this topic clearly requires further in depth investigation, it should be noted that in recent years, conformational flexibility has been proposed for several *meso*−carbon substituted porphyrins such as tetraalkylporphyrins due to hindered rotation of the *meso*−carbon substituents.[6a] The introduction of a significant ΔHOMO within the $[H_4TPTANP]^{2+}$ dication species due to the replacement of the central divalent metal with partial positive charges on four pyrrole nitrogen protons located, would account for the intensification of the Q_{00} band, Figures 5 and 6, and the reversal in the alignment of the induced magnetic moments and in the MCD sign sequences relative to ZnTPTANP.

Recent work by Ziegler, Baerends and co-workers on the calculation of Faraday $\mathcal{A}_1$ terms based on TD−DFT,[14] should eventually enable a quantitative DFT based approach to the analysis of the excited state magnetic properties of nonplanar peripherally crowded porphyrins to be carried out, similar to the semiempirical INDO/s based studies by Djerassi and co-workers[19a−c,37c] of chlorins, bacteriochlorins, isobacteriochlorins and monosubstituted free base porphyrins. The calculated $\mathcal{A}_1/\mathcal{D}_0$ ratios are currently found to be too low in comparison with experimentally derived values, due to a neglect of environment effects on the incident radiation and the relatively low accuracy of electric dipole strengths calculated by TD−DFT.[14] The oscillator strengths reported in Table 5 for the Q and B bands are consistently about a third to a half as intense as those obtained from INDO/s calculations based on the same set of B3LYP geometry optimizations. It should be noted that two close lying intense *x*/*y*-polarized $\pi \rightarrow \pi^*$ transitions of similar intensity were recently predicted in the B band region of ZnP and MgP by Baerends et al. based on statistical averaging of (model) orbital potentials (SAOP) calculations within the Amsterdam Density Functional package,[28k] Figure 9, which appears to be inconsistent with the available MCD spectral data,[7] Figure 5. Similar results are observed for the B band of ZnTPP based on B3LYP with 6−31G(d), Table 2, but not in the case of 6−31G basis sets and with INDO/s calculations, Table S2. Comparison of calculated and experimental magnetic moment values from the three Faraday terms would, therefore, provide an important additional spectroscopic basis for assessing the validity of DFT and TD−DFT based descriptions of the electronic structures and optical spectra of porphyrinoid complexes.

(b) Red Shifts of the Q and B Bands. Trends observed in the energies and intensities of the Q and B bands of a wide range of Zn(II) poprhyrinoids, Figures 7−10, 13, 14 are powerful tools with which to assess the impact of different structural modifications and to explore the reasons for the unusually large red shifts observed for both the Q and B bands of MTPTANP. Closed shell d^{10} metals such as Zn(II) or main group metal complexes are ideal candidates for studying trends in the energies of the Q and B bands since there are no ligand to metal or metal to ligand charge-transfer bands in the UV−visible region.[11] Previous research on TPTANP by Lash has focused largely on the role of fused−ring expansion with acenaphthalenes and ligand folding,[10] based on the valence bond model favored by organic chemists, rather than on the molecular orbital approach used in Gouterman's 4−orbital and in Michl's perimeter model. Lash pointed to the fact that partial peripheral fused ring substitution with fused acenaphthalenes results in a larger red shift of the B band than is the case with fused benzenes, naphthalenes and phenanthrenes, Figures 9 and 13.[10] TD−DFT and INDO/s calculations for a D_{4h} symmetry structure of ZnTPTANP predict a red shift of only 35−50 nm and 15−25 nm for the Q and B bands, respectively, Table 5. A brief inspection of Figures 9, 10, and 13 makes it clear that peripheral fused-ring ligand expansion and nonplanarity does not automatically result red shifts of ***both*** the Q and B bands. The main Faraday $\mathcal{A}_1$ term within the B band region of $Zn(\alpha C_6H_5)_8Pc$, a hard MCD chromophore with a saddled D_{2d} geometry, sits at 324 nm, despite a substantial red shift of the Q band to 780 nm,[18] Figure 10. When a structural perturbation, such as fused ring expansion or the introduction of aza-nitrogen, introduces a significant ΔHOMO, the ideal forbidden and allowed character

(37) (a) Keegan, J. D.; Bunnenberg, E.; Djerassi, C. *Spectrosc. Lett.* **1983**, *116*, 275−286. (b) Keegan, J. D.; Bunnenberg, E.; Djerassi, C. *Spectrochim. Acta A* **1984**, *40*, 287−297. (c) Goldbeck, R. A. *Acc. Chem. Res.* **1988**, *21*, 95−101.

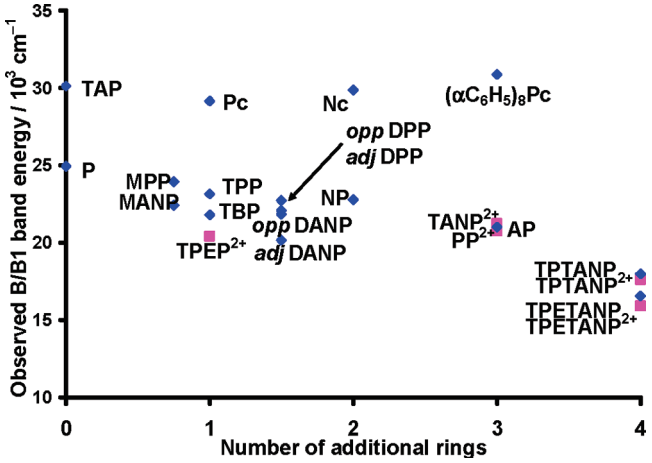

Figure 13. Observed B/B1 band energies plotted against the number of additional rings per pyrrole. Data points are included for H_4PP^{2+} and H_4-$TANP^{2+}$ dications (PP^{2+} and $TANP^{2+}$) and for the monosubstituted and opposite and adjacent disubstituted isomers of partially fused ring expanded PP complexes (MPP, *adj*DPP and *opp*DPP) and TANP complexes (MANP, *adj*DANP, and *opp*DANP) reported by Lash[10] as well as for the meso-tetraphenylethynylporphyrin dication ($TPEP^{2+}$) reported by Milgrom and Yahioglu.[50] Dication species are indicated with square magenta symbols.

of the Q and B bands is lost and the Q−B band separation increases, Figures 8−10 and Tables 2, 5, and 6. The B1 and B2 bands of ligands such as ZnPc,[8,12,34] are located significantly to the blue of the B band of ZnP due to configuration interaction between the B and higher energy $\pi\pi^*$ states which are not included within Gouterman's 4-orbital and in Michl's perimeter model, Tables 2, 5, and 6, Figure 13, while in contrast the Q band red shifts and intensifies. The unusually large red shifts reported by Lash[10] for ***both*** the Q_{00} and B_{00} bands of ZnTP-TANP are, therefore, along with the anomalous negative Faraday $\mathscr{A}_1$ terms, the result of the ligand being a double-soft MCD chromophore with optical properties similar to an ideal $C_{16}H_{16}^{2-}$ perimeter ($\alpha \approx 0°$) since ΔHOMO, ΔLUMO ≈ 0. In addition, TD−DFT and INDO/s based calculations predict that the HOMO−LUMO band gap is reduced significantly in the case of acenaphthalene fused-ring-expanded ligands, thus accounting for part of the unprecedented red shift of the B band of ZnTPTANP, Figure 13.[10] Although this trend is not as marked in the INDO/s calculations, this is due primarily to a difference in the predicted band intensities for TATANP, Figure 9.

Michl[15] has demonstrated that the observed Q_{00} and B_{00} band intensities and wavelength properties of structurally modified porphyrinoid can be related back to those of an ideal D_{nh} symmetry C_nH_n perimeter since the nodal patterns of π−MOs are retained even after the symmetry is lowered, Figure 15 and S1. The marked differences in the electronic and optical properties observed in Figures 7−10, 13, and 14 are related to the fact that the acenaphthalene fused-ring-expansions contain a 12 π−electron system based on part of the repeating unit of C_{60}, while in contrast the fused six membered rings on the periphery of TBP, TPTBP, Pc, NP, TPTNP, Nc, Ac, and AP involve 6, 10, or 14 π−electrons based on expansion with the repeating unit of graphite through expansion with benzenes, naphthalenes or anthracenes. A significant ΔHOMO is introduced, in the case of the graphite based fused-ring expansions since the $1a_{1u}$ MO is destabilized more significantly than the $1a_{2u}$ MO, Figure 15, since the alternating nodal pattern of the $1a_{1u}$ MO is repeated in a set of minor nodes on the outer ligand perimeter as well as the inner perimeter. In contrast, the nodal patterns of the $1a_{2u}$ MO remain located primarily on the inner perimeter due to the interaction between the metal and the nodes on the four pyrrole nitrogens. No significant destabilization of the $1a_{1u}$ MO would be anticipated in the case of ZnTANP, however, since a fully alternating nodal pattern on the outer perimeter would result in a set of nodes on a pair of 2-fold axes within the *xy*-plane, which is forbidden for symmetry reasons.

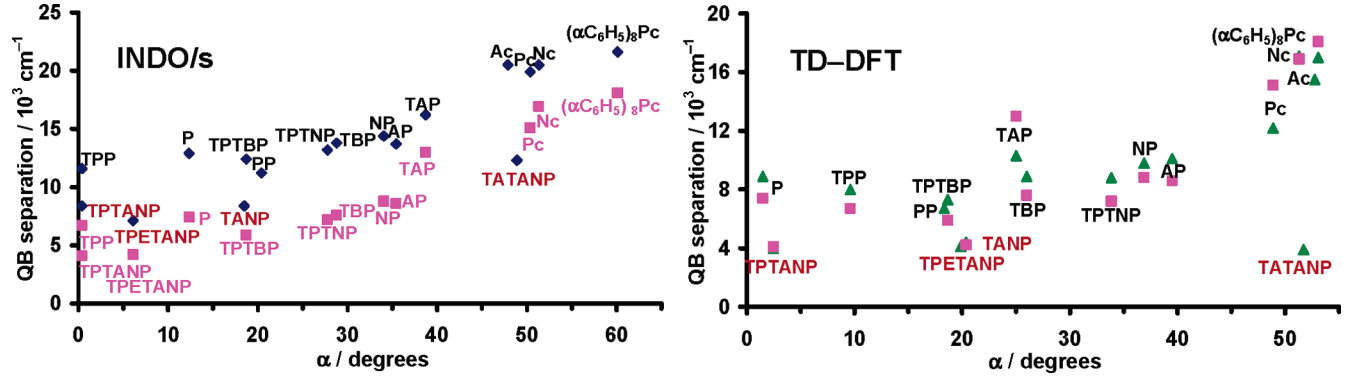

Figure 14. Experimentally observed (magenta squares) and calculated (blue diamonds and green triangles), Table 5, energy separation of the Q and B bands against plotted the degree of mixing of the Q and B excited-state magnetic moments(α) derived from the oscillator strengths predicted by INDO/s (LEFT) and TD−DFT (RIGHT) calculations based on geometry optimizations obtained with the B3LYP functional with 6−31G basis sets.

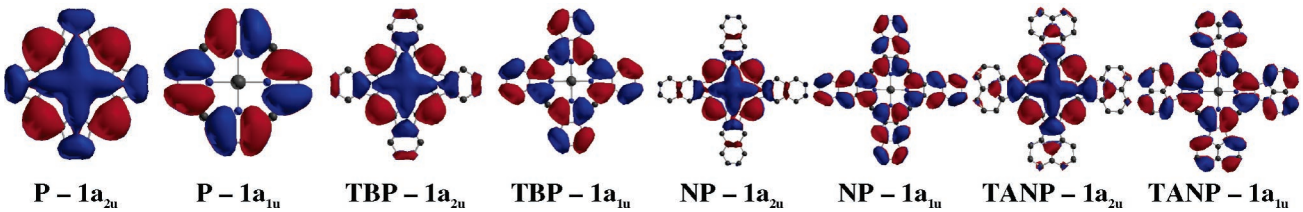

Figure 15. Two π-HOMOs of ZnP, ZnTBP, ZnNP, ZnAP, and ZnTANP based on Gaussian checkpoint files using CS Chem 3D with an electrostatic potential isosurface of 0.01 au. Plots for the same MOs at an isosurface of 0.035 au showing only the major nodes are provided in Figure S5.

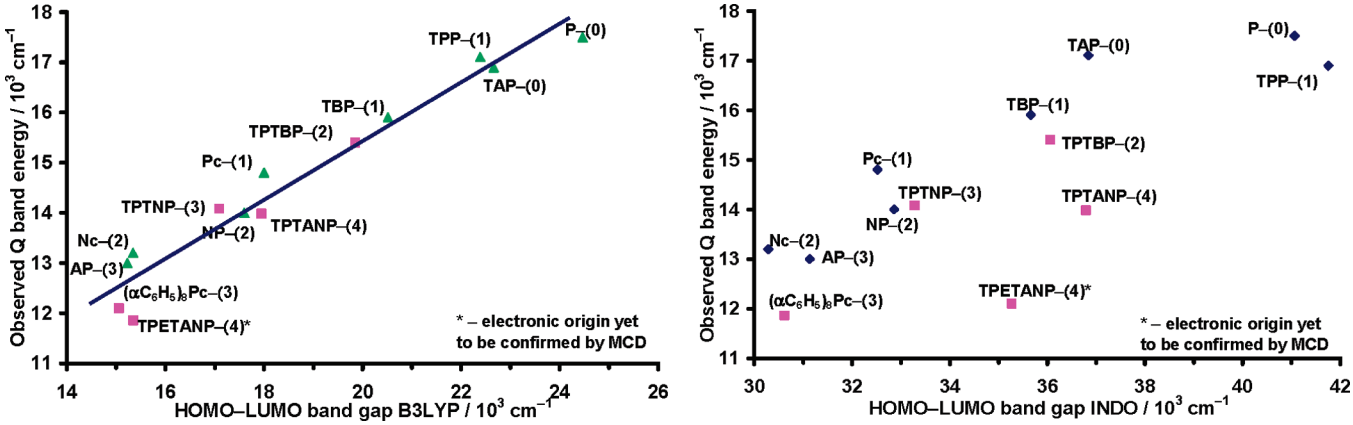

Figure 16. Observed Q band energy plotted against the calculated HOMO−LUMO band gap from B3LYP calculations with 6−31G basis sets, Figure 4. The number of additional rings per pyrrole is indicated for each complex. Saddled S_4 or D_{2d} geometry complexes are indicated with magenta squares.

(c) Importance of Substituent Effects. There has been considerable recent controversy over the cause of significant red shifts observed in the major UV−visible absorption bands of peripherally crowded dodecasubstituted porphyrins.[6a,b,e−1,9] Shelnutt and co-workers have proposed, based on molecular mechanics calculations, that there is a direct correlation between the red shifts observed for the Q_{00} and B_{00} bands of sterically hindered porphyrins and the degree of ligand nonplanarity.[2,6] In contrast, di Magno has pointed to substituent effects as the major cause cause based on in-plane nuclear reorganization.[9b−d] The trends observed in Figures 7−10, 13, and 14 for a wide range of porphyrinoid ligands demonstrate that structural perturbations to the ligand perimeter at the *meso*-carbon positions, such as phenylation and aza-substitution, play a key role in determining the wavelengths and relative intensities of the main $\pi \rightarrow \pi^*$ bands, due to the fact that major nodes of the $1a_{2u}$ MO are located at the *meso*-carbons, Figure S1. There is a marked red shift of the Q and B bands of TPETANP relative to TPTANP,[10] Figures 9 and 10, despite the ligand being predicted to be saddled to almost the same degree by B3LYP geometry optimizations, Table 1. This represents evidence that substituent effects can play an important role in determining the extent of the evidence for a correlation between the degree of ligand nonplanarity and the magnitude of red shifts observed for both the Q and B bands in the spectra of sterically hindered porphyrins, in our opinion the S_4 symmetry, saddled and ruffled porphyrins used would only be valid for modeling porphyrin nonplanarity in proteins in instances where the protein environment results in the formation of a high-symmetry soft MCD chromophore, which retains a 4-fold axis of symmetry. Asymmetrical structural perturbations that introduce a significant ΔHOMO and/or ΔLUMO could result in significant configurational interaction between the B and higher energy $\pi\pi^*$ excited states and a red and blue shift of the Q and B bands, respectively, in line with the trends observed for hard MCD chromophores in Figures 7−10, 13, and 14. In the case of B3LYP calculations the observed Q band wavelengths for the saddled TPTANP and TPETANP complexes are consistent with the general trend for Q band wavelength plotted against the predicted HOMO−LUMO band gap, Figure 16. In contrast, there is a marked deviation in the case of INDO/s calculations based on the same set of structures obtained from B3LYP geometry optimizations. Since trends based on the wavelengths of the Q_{00} and B_{00} band predicted by INDO/s have been used extensively within Shelnutt's studies, the influence of the degree of nonplanarity on the accuracy of results obtained from INDO/s calculations may need to be carefully assessed.

Conclusions

In contrast with other structurally modified porphyrinoids, such as ZnTBP and ZnPc, the inner perimeter of ZnTPTANP is a soft MCD chromophore since ΔHOMO, ΔLUMO ≈ 0. The Q and B bands, therefore, maintain their fully forbidden and allowed character, respectively. The MCD spectrum of ZnTPTANP is dominated by negative Faraday $\mathcal{A}_1$ terms due to significant saddling of the ligand to form an S_4 symmetry structure. Saddling quenches OAM within the LUMO to a greater extent than within the HOMOs, since electron density extends beyond the inner perimeter to a greater extent. The relative lack of configuration interaction between the B and higher energy $\pi\pi^*$ states in the case of soft MCD chromophores and a reduced energy separation between the Q and B excited states associated with the fused-ring-expansion of the porphyrin ligand with acenaphthalenes are the primary reasons for the remarkably large red shifts of the B (or Soret) band that was reported by Lash.[10] The analysis of the ZnTPTANP MCD spectrum illustrates the continuing value of Gouterman's 4-orbital LCAO[7,16] and Michl's perimeter model[15] for studying the electronic structure of heteroaromatic complexes. The unusual optical spectroscopic properties observed for ZnTPTANP suggest that studies of the acenaphthoporphyrins will lead to significant new chemical properties based on the structural properties of the porphyrinoid ligand, much like the many successes, in recent years, within studies of the corroles[38] and tetraazaporphyrins.[39]

(38) (a) Paolesse, R. In *The Porphyrin Handbook*; Kadish, K. M., Smith K. M., Guilard, R., Eds.; Academic Press: London, 2000; Vol. 2, Ch. 11, pp 201−231. (b) Erben, C.; Will, S.; Kadish, K. M. In *The Porphyrin Handbook*; Kadish, K. M., Smith K. M., Guilard, R., Eds.; Academic Press: London, 2000; Vol. 2, Ch. 11, pp 232−300.
(39) Kobayashi, N. In *The Porphyrin Handbook*; Kadish, K. M., Smith K. M., Guilard, R., Eds.; Academic Press: London, 2000; Vol. 2, Ch. 13, pp 301−360.
(40) Eisner, U.; Linstead, R. P. *J. Chem. Soc.* **1955**, 3749−3754.
(41) Linstead, R. P.; Whalley, M. *J. Chem. Soc.* **1952**, 4839−4846.
(42) Barnett, G. H.; Hudson, M. F.; Smith, K. M. *J. Chem. Soc., Perkin Trans. 1* **1975**, 1401−1403.
(43) Gouterman, M. *J. Mol. Spectrosc.* **1961**, *6*, 138−63.
(44) Whalley, M. *J. Chem. Soc.* **1961**, 866−869.
(45) Kopranenkov, V. N.; Daskevich, S. N.; Luk′yanets, E. A. *Zh. Obsch. Khim.* **1979**, *49*, 1408−1412.
(46) Kopranenkov, V. N.; Vorotnikov, A. M.; Daskevich, S. N.; Luk′yanets, E. A. *Zh. Obsch. Khim.* **1985**, *54*, 1408−1412.

Acknowledgment. We thank NSERC of Canada for Operating and Equipment grants (to M.J.S.), support from Fujitsu America Inc. in providing the CAChe Workstation software and Sharcnet, University of Western Ontario for access. This research was partially supported by the Japanese Ministry of Education, Science, Sports and Culture, a Grant-in-Aid for the COE project, Giant Molecules and Complex Systems, 2005, and from Grant-in-Aid for Scientific Research (B) No. 17350063 (to N.K.). M.J.S. is a member of the Centre for Chemical Physics at UWO.

Supporting Information Available: Additional theoretical background to MCD spectroscopy, nodal patterns for the frontier p-MOs and calculated UV−visible absorption spectra of the porphyrinoids in Table 2 based on Gaussian checkpoint files and the Tabulator program of the CAChe workstation, additional tables for geometry of central ligand cavities predicted by B3LYP, calculated spectra and MO energies of ZnP, ZnTPP, ZnTANP, and ZnTPTANP, band deconvolution parameters for ZnTPTANP and $[H_4TPTANP]^{2+}$, and MO energies and eigenvectors predicted for the major bands of the porphyrinoids in Table 2. This material is available free of charge via the Internet at http://pubs.acs.org.

JA0540728

(47) Kobayashi, N.; Mack, J.; Ishii, K.; Stillman, M. J. *Inorg. Chem.* **2002**, *41*, 5350−5363.
(48) (a) Numao, M. M. Sc. Thesis, Tohoku University 1991. (b) Kobayashi, N.; Nevin, W. A.; Mizunuma, S.; Awaji, H.; Yamaguchi, M. *Chem. Phys. Lett.* **1993**, *205*, 51−54.
(49) Kobayashi, N.; Nakajima, S.-i.; Ogata, H.; Fukuda, T. *Chem. Eur. J.* **2004**, *10*, 6294−6312.
(50) Milgrom, L. R.; Yahioglu, G. *Tetrahedron Lett.* **1995**, *36*, 9061−9064.